

AD-A034 451

PENNSYLVANIA STATE UNIV UNIVERSITY PARK APPLIED RESE--ETC F/G 20/1
QUANTITATIVE SCHLIEREN VISUALIZATION.(U)

OCT 76 S STANIC

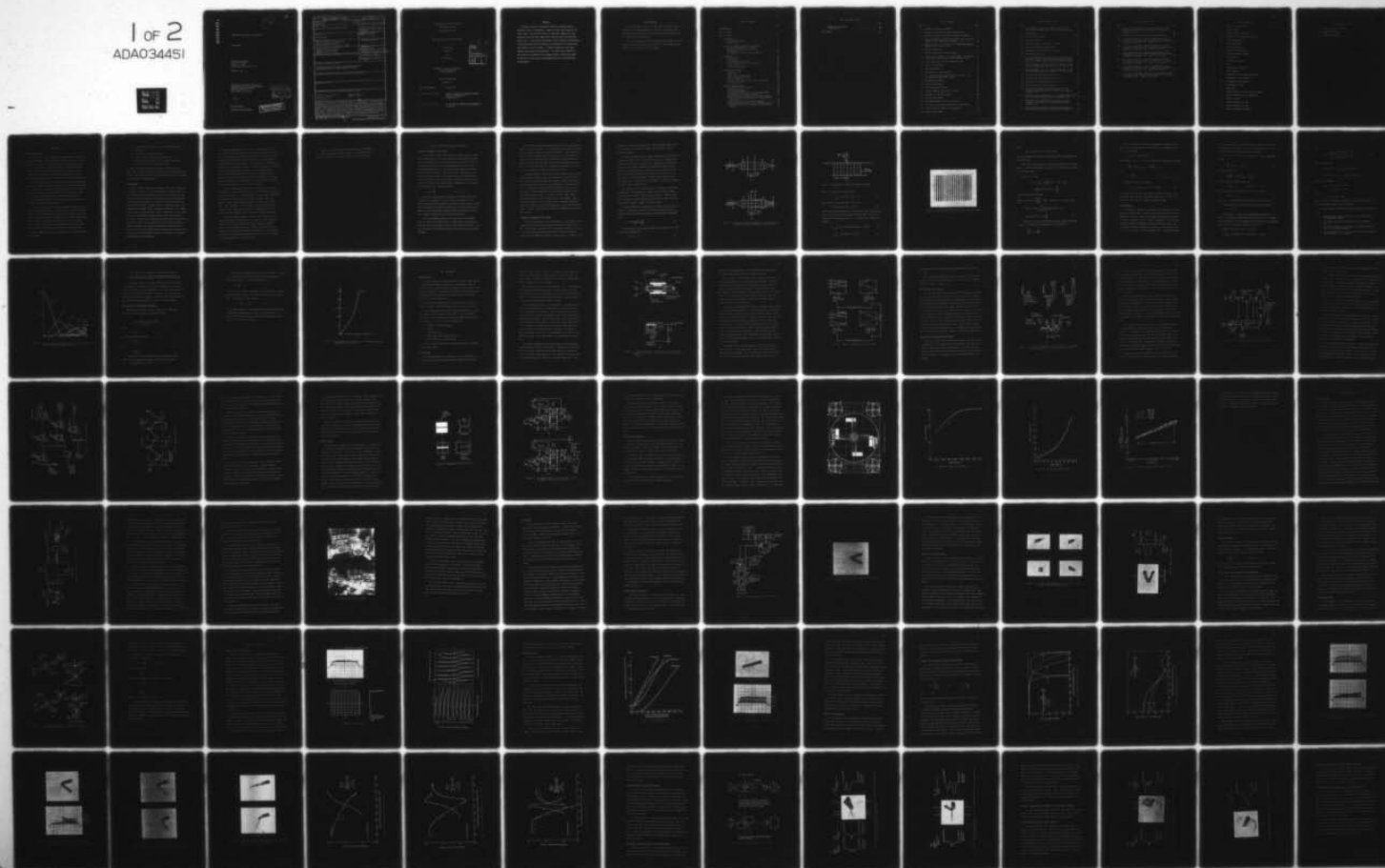
N00017-73-C-1418

UNCLASSIFIED

TM-76-279

NL

1 of 2
ADA034451



ADA034451

12

F.C.

QUANTITATIVE SCHLIEREN VISUALIZATION

Steve Stanic

Technical Memorandum
File No. TM 76-279
October 1, 1976
Contract No. N00017-73-C-1418

Copy No. 6

The Pennsylvania State University
Institute for Science and Engineering
APPLIED RESEARCH LABORATORY
Post Office Box 30
State College, PA 16801

APPROVED FOR PUBLICATION
DIS. UNLIMITED

NAVY DEPARTMENT
NAVAL SEA SYSTEMS COMMAND

DDC
RECEIVED
JAN 17 1977
A

DISTRIBUTION STATEMENT A
Approved for public release;
Distribution Unlimited

REPORT DOCUMENTATION PAGE		READ INSTRUCTIONS BEFORE COMPLETING FORM
1. REPORT NUMBER TM-76-279	2. GOVT ACCESSION NO.	3. RECIPIENT'S CATALOG NUMBER <i>Internal thesis</i>
4. TITLE (and Subtitle) QUANTITATIVE SCHLIEREN VISUALIZATION		5. TYPE OF REPORT & PERIOD COVERED Ph.D. Thesis, March 1977
7. AUTHOR(s) Steve Stanic		6. PERFORMING ORG. REPORT NUMBER TM 76-279
9. PERFORMING ORGANIZATION NAME AND ADDRESS The Pennsylvania State University Applied Research Laboratory P. O. Box 30, State College, PA 16801		8. CONTRACT OR GRANT NUMBER(s) N00017-73-C-1418
11. CONTROLLING OFFICE NAME AND ADDRESS Naval Sea Systems Command Department of the Navy Washington, D. C. 20362		10. PROGRAM ELEMENT, PROJECT, TASK AREA & WORK UNIT NUMBERS <i>1 Oct 76</i>
14. MONITORING AGENCY NAME & ADDRESS (if different from Controlling Office)		12. REPORT DATE October 1, 1976
		13. NUMBER OF PAGES 108 pages & figures <i>110p.</i>
		15. SECURITY CLASS. (of this report) Unclassified, Unlimited
		15a. DECLASSIFICATION/DOWNGRADING SCHEDULE
16. DISTRIBUTION STATEMENT (of this Report) Approved for public release, distribution unlimited, per NSSC (Naval Sea Systems Command) 11/22/76		
17. DISTRIBUTION STATEMENT (of the abstract entered in Block 20, if different from Report)		
18. SUPPLEMENTARY NOTES		
19. KEY WORDS (Continue on reverse side if necessary and identify by block number) Sound pressure measurement Signal processing Schlieren systems Acoustic beams Video signals		
20. ABSTRACT (Continue on reverse side if necessary and identify by block number) A method to obtain quantitative information directly from a Schlieren image is investigated. Using the exact timed format of the video signal, the television raster is vertically scanned at a predetermined position and a sample point taken on each of the 525 horizontal lines. Using digital techniques, voltage displays corresponding to the black-white scene information are presented on an oscilloscope and plotted on an X-Y recorder. A single calibration curve gives relative sound pressure measurements. The results are compared for high frequency transmission and reflection from a thick steel plate. In addition, optimum optical arrangements and source configurations are discussed.		

The Pennsylvania State University

The Graduate School

Department of Physics

Quantitative Schlieren Visualization

A Thesis in

Physics

by

Steve Stanic

DATE	WRITE DATE
DDC	DATE
EXAMINER	
JUSTIFICATION	
BY	
DISTRIBUTION/APPROPRIATE CODES	
RECEIVED	DATE
SPECIAL	

Submitted in Partial Fulfillment
of the Requirements
for the Degree of

Doctor of Philosophy

March 1977

Date of Signature:

Signatories:

Eugen J. Skudrzyk, Professor of Physics
Chairman of Committee
Thesis Adviser

R. H. Good, Jr., Head of the Department
of Physics

ABSTRACT

A method to obtain quantitative information directly from a Schlieren image is investigated. Using the exact timed format of the video signal, the television raster is vertically scanned at a predetermined position and a sample point taken on each of the 525 horizontal lines. Using digital techniques, voltage displays corresponding to the black-white scene information are presented on an oscilloscope and plotted on an X-Y recorder. A single calibration curve gives relative sound pressure measurements. The results are compared for high frequency transmission and reflection from a thick steel plate. In addition, optimum optical arrangements and source configurations are discussed.

ACKNOWLEDGMENTS

The author wishes to express his gratitude to Professor Eugen J. Skudrzyk for his guidance and support and to Mr. Lynn Poole of the Development Engineering Group at the Applied Research Laboratory of The Pennsylvania State University.

This work was supported by the Applied Research Laboratory of The Pennsylvania State University and the Office of Naval Research under contract with the Naval Sea Systems Command.

TABLE OF CONTENTS

	Page
ACKNOWLEDGMENTS	11
LIST OF FIGURES	v
LIST OF SYMBOLS	viii
I. INTRODUCTION	1
Purpose of the Study	1
Previous Work	2
II. THEORY OF LIGHT DIFFRACTION BY ULTRASOUND	5
Different Treatments of the Theory	5
A Simplified Treatment of the Theory	6
The Parameter Q	12
The Variable ν (the Raman-Nath Parameter)	16
III. ELECTRONICS	19
Imaging System	19
Vidicon Tube	19
The Composite Video Signal	24
Analysis of the Composite Video Signal	24
Target Voltage	32
Vidicon Tube Parameters	35
IV. THE SCHLIEREN SYSTEM	42
Schlieren Setup	42
Transducers	48
Various Modes of Operation	49
Format of the Output Signal	52
Critical Constants	55
The Slit versus the Pinhole as the Light Source	55
Low Frequency Limit	56
V. RESULTS AND DISCUSSION	59
Vidicon Surface Characteristics	59
Calibration Curves	62
Vidicon Tube Parameters	65
An Example of Quantitative Schlieren Measurements	66
Three-Dimensional Schlieren Information	77
Diffraction and Transmission for an Aluminum Wedge	77
Acoustic Transmission and Reflection from Concentric Cylinders	81
Spectral Reflection from a Prolate Spheroid	81
Transmission and Reflection from a Welded Steel Plate	84
A Ribbed Steel Plate Insonified by a Short Acoustic Pulse	84

Table of Contents (cont.)

	Page
VI. SUMMARY AND CONCLUSIONS	93
Future Work	94
BIBLIOGRAPHY	96

LIST OF FIGURES

Figure	Page
1. Schematic of optical arrangement	8
2. Diagram of the ultrasonic diffraction grating	9
3. Typical photograph of ultrasonic diffraction spectra	10
4. Light intensities of several Fraunhofer orders versus the variable v under Raman-Nath conditions	15
5. Image intensity as a function of the Raman-Nath parameter (Smirnov et al., 1973, p. 160)	18
6. Vidicon camera tube	21
7. Odd-line interlaced scanning procedure	23
8. (a) The three components of a video signal. (b) Composite video signal for three consecutive horizontal lines	25
9. Circuit description of the transient recorder	27
10. Vidicon scan controller	29
11. Sampling procedure	30
12. Representative vertical output	33
13. (a) Original Vidicon light sensitivity circuit. (b) Modified light sensitivity circuit	34
14. Standard test pattern	37
15. Image size resolution	38
16. Vidicon dark current noise	39
17. Vidicon transfer characteristic curves	40
18. Schematic of Schlieren system	43
19. The Schlieren system	46
20. Instrument setup for Schlieren system	50
21. Continuous acoustic beam incident on a steel plate	51
22. A 20- μ sec pulse incident on a steel plate	53
23. Output signal format	54

List of Figures (cont.)

Figure	Page
24. (a) Diffraction orders for a pinhole light source. (b) Diffraction orders for a vertical slit light source .	57
25. Vidicon grid	60
26. Vidicon response curves	61
27. Calibration curves	63
28. Schlieren image of a continuous 5.38 Mhz	64
29. Reflectivity (Mindlin plate theory)	67
30. Transmission loss (Mindlin plate theory)	68
31. Horizontal video signal	70
32. (a) Schlieren image of a steel plate insonified by 4.62 Mhz acoustic beam. (b) Horizontal video signal display showing uniform incident and reflected intensity levels .	71
33. Schlieren images of a steel plate insonified at 5.3 Mhz and at different angles of incidence: (a) 30°; (b) 40° .	72
34. Schlieren images of a steel plate insonified at 5.3 Mhz and at different angles of incidence: (a) 50°; (b) 65° .	73
35. Reflection and transmission loss for $\Omega = 1$	74
36. Reflection and transmission loss for $\Omega = 1.35$	75
37. Reflection and transmission loss for $\Omega = 2.1$	76
38. Three-dimensional Schlieren system	78
39. Reflection, transmission and diffraction for a 60° aluminum wedge insonified at 4.62 Mhz with the angle of incidence = 10°	79
40. Reflection and transmission for a 60° aluminum wedge inson- ified at 4.62 Mhz with the angle of incidence = 30°	80
41. Reflection and transmission for concentric aluminum cylinders insonified at 4.62 Mhz with the angle of incidence = 35°	82
42. Spectral reflection from an aluminum prolate spheroid insonified at 4.62 Mhz with the angle of incidence = 20° .	83

List of Figures (cont.)

Figure	Page
43. Reflection and transmission for two steel plates welded together and insonified at 4.62 Mhz with the angle of incidence = 15°	85
44. Calibration curve for a 30- μ sec long 4.62 Mhz pulse . . .	86
45. A thin steel plate with a steel rib welded on one side insonified by a 30- μ sec long, 4.62 Mhz acoustic pulse with the angle of incidence = 15° . Time = T_1	87
46. A thin steel plate with a steel rib welded on one side insonified by a 30- μ sec long, 4.62 Mhz acoustic pulse with the angle of incidence = 15° . Time = $T_1 + 10 \mu$ sec	88
47. A thin steel plate with a steel rib welded on one side insonified by a 30- μ sec long, 4.62 Mhz acoustic pulse with the angle of incidence = 15° . Time = $T_1 + 20 \mu$ sec	89
48. A thin steel plate with a steel rib welded on one side insonified by a 30- μ sec long, 4.62 Mhz acoustic pulse with the angle of incidence = 15° . Time = $T_1 + 30 \mu$ sec	90
49. A thin steel plate with a steel rib welded on one side insonified by a 30- μ sec long, 4.62 Mhz acoustic pulse with the angle of incidence = 15° . Time = $T_1 + 40 \mu$ sec	91
50. A thin steel plate with a steel rib on one side insonified by a 30- μ sec long, 4.62 Mhz acoustic pulse with the angle of incidence = 15° . Time = $T_1 + 50 \mu$ sec	92

LIST OF SYMBOLS

b	width of the opaque stop
c	speed of light
c'	speed of sound in the medium
d_n	separation of the diffraction orders
\vec{E}	electric field vector
F	lens focal length
f	sound beam frequency
L	width of the sound field
n	diffraction order component
P	sound pressure
R	reflection coefficient
t	time
T	transmission coefficient
Z	plate impedance
λ^*	wavelength of the incident sound beam
λ	wavelength of the light beam
k^*	wavenumber for ultrasound
k	wavenumber for light
δ_j	phase angle
θ	angular position of the diffraction orders
$\bar{\theta}$	angle of incidence of the light beam
ρ	density of water
ω^*	angular frequency of sound
ω	angular frequency of light
ω'	angular coincidence frequency

List of Symbols (cont.)

ω_0 plate coincidence frequency

u_0, u_j index of refraction

v, v_j Raman-Nath parameter

I. INTRODUCTION

Purpose of the Study

One problem that has become increasingly important is the interaction of underwater acoustic waves with complex structures. In past investigations acoustic intensity data have been obtained by hydrophones. In effect this technique measures the sound pressures at individual points in a sound field. In order to obtain an understanding of the complexity of an interacting sound field, a large number of measurements have to be taken and the results interpolated.

It has become very costly to conduct these large-scale experiments and efficient planning is only possible if the investigator knows what he is searching for. Thus model experiments have become very valuable and in most instances provide investigators with an accurate visual picture of the phenomenon under study. Model experiments using Schlieren methods have become increasingly useful since these require a minimum of preparation and expenditure.

This thesis describes an investigation aimed at the utilization of the acoustic Schlieren system as a sensitive tool to visualize complex sound fields. An additional objective was the development of a method to quickly obtain quantitative information on the pressure distributions directly from a Schlieren image without the use of films or photomultiplier tubes. It should be noted however, that this thesis does not deal with the theoretical background of the Schlieren system.

Acoustic interactions which lend themselves to visual experimental methods include:

1. Reflection and transmission of acoustic beams by plates
2. Diffraction
3. Transmission through welded joints
4. Acoustic effects of plates with welded ribs
5. Transmission and reflection from concentric cylinders
6. Acoustic scattering by prolate spheroids.

The above are complex interactions which do not easily yield to analytical treatments, and in many cases even qualitative knowledge is lacking. Thus these interactions have become ideal topics for analysis by an acoustical Schlieren system.

Previous Work

Early literature provides many examples of the uses of Schlieren techniques. Following its initial development by Toppler (1867), the Schlieren method has been used extensively in the research of high-speed gas flows and applications in the study of acoustical problems dates back to the mid 1930's. Since then, the Schlieren method has been used by Bär (1936), Giacomini (1938), Hiedemann and Hoesch (1937), Hiedemann and Ostermmel (1937), Parthasarthy (1936a,b), Seidl (1948), Willard (1949), Barnes and Burton (1949), Straub (1947), Barone (1950), and others in the study of problems ranging from vibrating quartz crystals to reflection and transmission from numerous complex structures. [An outline of many of these publications can be found in Bergmann (1954)]. Typically, these studies describe the standard Schlieren setup, but they do not contain discussions relative to the construction of the system for optimum efficiency, nor do they make any attempt to gather quantitative information.

Neubauer and Dragonette (1970) have conducted perhaps the most noted recent research in acoustical Schlieren visualization. By using Schlieren photographs and motion pictures, they identified the various circumferential and surface creeping waves that are generated by a cylinder which has been insonified. Later, Dragonette (1972) used the same method to study sound transmission through thin plates. Schlieren method enabled Neubauer and Dragonette (1973) to demonstrate the existence of Rayleigh waves and to calculate their phase velocity. However, intensity measurements made by these researchers were accomplished through the use of hydrophones. They also made little effort to discuss the qualities of their Schlieren system.

Efforts to gather quantitative data directly from a Schlieren image have not been altogether successful. Most attempts are reported in Russian literature. In most instances, the quantitative information was gathered through the use of photometry. Korolev (1937) and Bazhulin (1948) used the method to measure the absorption of sound waves in air and water. In these studies, it was assumed that the sound and light intensities were linearly related and it was this assumption that cast doubt on the reliability of their measurements.

In a recent paper by Smirnov, Kheifets, and Shenderov (1973), a quantitative method is described which, although it uses photometry, takes into account the nonlinear relationship between the sound pressure and the image illumination. However, this method does not enable quick and reliable quantitative determinations. In addition, problems exist with the film calibration and the critical development requirements needed for consistent results.

Finally, a study of Bucaro, Flax, and Dardy (1976) attempted to use computer-generated intensity functions and a photomultiplier-pinhole recording device to obtain quantitative Schlieren data.

II. THEORY OF LIGHT DIFFRACTION BY ULTRASOUND

Different Treatments of the Theory

In 1932, Debye and Sears described an experiment in which a plane beam of monochromatic light from a distant slit was normally incident on a fluid-filled cell. The conditions were such that the medium was homogeneous and isotropic, thus allowing the beam of light to pass undeviated through the cell. The cell was then normally traversed by high-frequency sound waves. The result was a stratification of the fluid into regions of varying refractive index. The light emerging from the cell consisted of various beams traveling in different directions with respect to the incident beam. Experimentally it was found that these beams were at angles given by:

$$\sin \theta = \frac{N\lambda}{\lambda^*} \qquad N = 0, 1, 2, 3, \dots$$

Since this initial discovery, numerous investigations have been undertaken in an attempt to clarify the above observations. The earliest comprehensive treatment was by Raman and Nath (1935a,b, 1936a,b) which described the phenomenon by considering the high-frequency sound beam as a phase grating and pictured the diffracted light in terms of phase changes incurred while traversing the sound beam.

Since the Raman-Nath publications there has been considerable effort to add to the original theory. In many cases, the methods are much more sophisticated making use of new and advanced techniques. Ray and phase theories have been developed and exact methods of integration attempted.

In 1951 Nomoto presented a geometrical theory of light diffraction. However, due to the nature of the approximations he was able to produce only the broadest features of the exact treatments. Later, Nomoto and Negishi (1965) devised an analytical expression for the intensity distribution of the diffracted spectra produced by a sawtooth waveform. Bhatia and Noble (1953) presented a most interesting approach to ultrasonic light diffraction when they formulated the problem into a series of integral equations and used a perturbation solution.

Hiedemann and Zankel (1961) discuss the different methods by which the waveforms of ultrasonic waves in liquids may be studied. Klein, Cook, and Mayer (1965) formulated this problem in terms of difference-differential equations and used these equations for numerical evaluations. In addition, a general geometric treatment can be found in Born (1965). Further examination of the literature reveals numerous other relevant publications. For example, Willard (1949), Quate, Wilkinson, and Winslow (1965), Klein, Tipnis, and Hiedemann (1965), Kang and Young (1972), Pierce and Byer (1973), and Neeson and Austin (1975) all attempt to reveal different aspects of the light diffraction theory. Finally, a book by Berry (1966) deals comprehensively with the same subjects.

A Simplified Treatment of the Theory

For this investigation it is assumed that the sound pressure field produced in the fluid cell originates from a purely sinusoidal plane wave. Specifically, this means that the transducer operates in or close to its linear region and this source produces a purely sinusoidal variation of the index of refraction in the fluid cell. Further, it is

assumed that the waves are progressive. With the present state of the art of transducer and electronic design, these conditions are not difficult to achieve.

A typical arrangement for the study of ultrasonic light diffraction is shown in Figures 1 and 2. The light source, S1, is focused by the condensing lens, L1, onto the pinhole P1. After passing through the pinhole the light beam is expanded, collimated and allowed to pass through the fluid-filled cell. The light is then focused by lens L3 onto a glass plate located at the focal point of the last lens. For the purposes of Schlieren imaging, a spatial filter located on the glass plate, S2, is used to block out the image of the light (discussed in greater detail in Chapter IV).

The transducer, T1, is located so that it produces a sound field perpendicular to the light beam. Without the sound beam, the only image on the glass plate is that of the light source. However, when the sound beam is present a Fraunhofer diffraction pattern, similar to that shown in Figure 3, appears on the glass plate.

The wave equation which describes the propagation of the electric field in a region free of current and charge and where the index of refraction varies slowly with distance, can be written as (Skudrzyk, 1971):

$$\nabla^2 \vec{E} = \frac{[\mu(x,t)]^2}{c^2} \frac{\partial^2 \vec{E}}{\partial t^2} . \quad (1)$$

The variation of the refractive index in the region of the sound field can be expressed as:

$$\mu(x,t) = \mu_0 + \mu' , \quad (2)$$

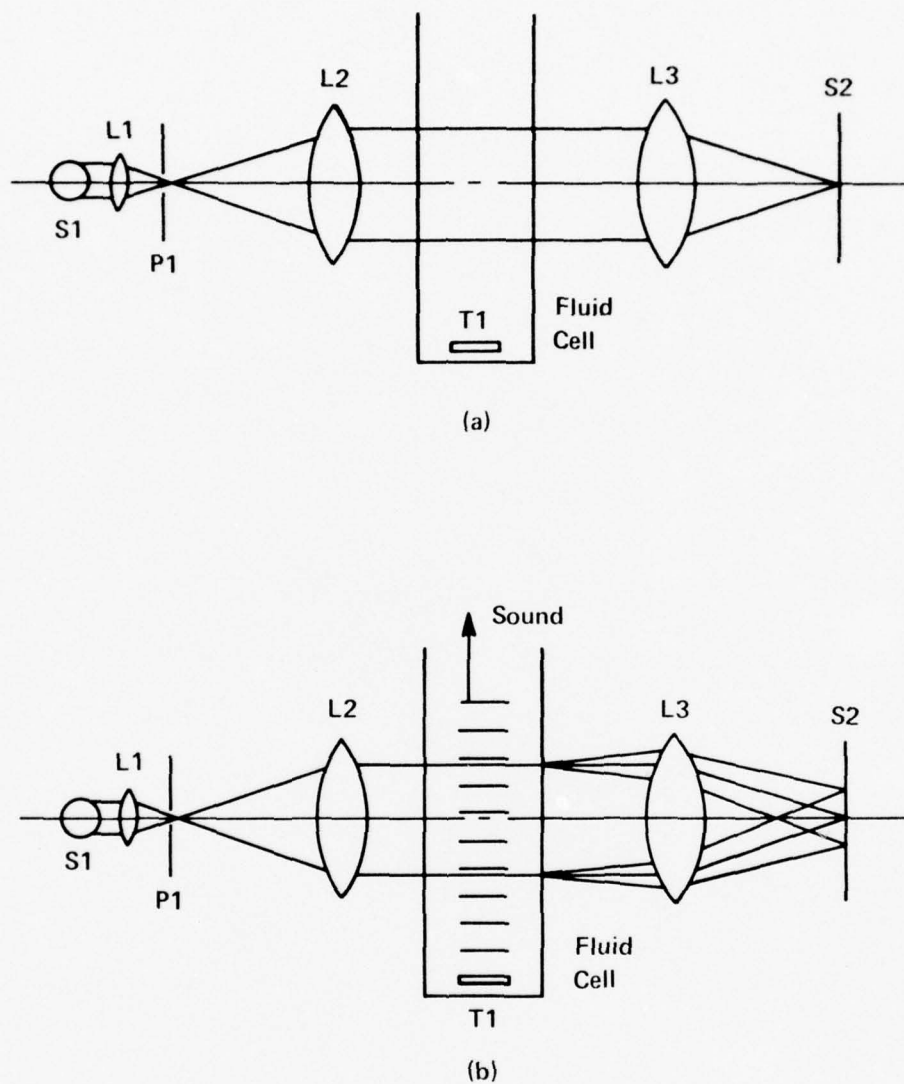


Figure 1. Schematic of optical arrangement. (a) Sound beam off. (b) Sound beam on with diffraction orders present.

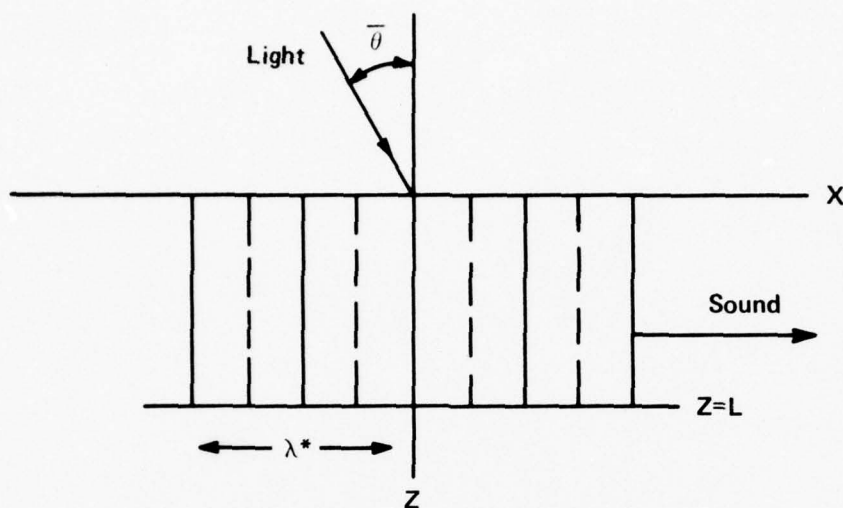


Figure 2. Diagram of the ultrasonic diffraction grating.

where μ' is given by the Fourier series

$$\mu' = \sum_{j=1}^{\infty} \mu_j \sin[j(\omega^* t - k^* x) + \delta_j] \quad (3)$$

The solution can then be written in the form:

$$E = \psi(x, z, t) \exp i(\omega t - \mu_0 \vec{k} \cdot \vec{r}) \quad (4)$$

where the exponential describes the propagation of the light beam and $\psi(x, z, t)$, the effect of the sound on the light beam. Then, representing the x -direction variation as a Fourier series, equation (4) becomes:

$$E = \sum_{n=-\infty}^{\infty} \xi_n(z, t) \exp[-in k^* x] \exp[i(\omega t - \mu_0 \vec{k} \cdot \vec{r})] \quad (5)$$

$$= \sum_{n=-\infty}^{\infty} \xi_n(z, t) \exp[i(\omega t - \vec{k}_n \cdot \vec{r})] \quad (6)$$

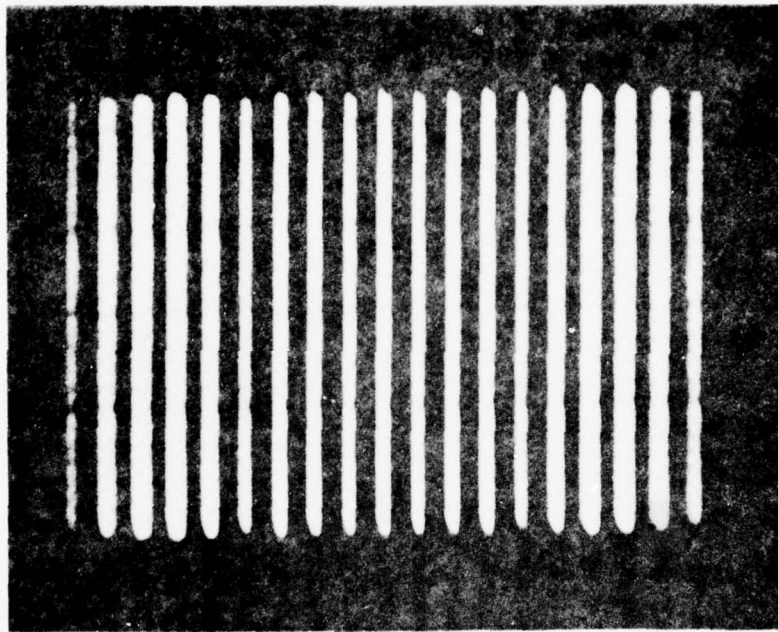


Figure 3. Typical photograph of ultrasonic diffraction spectra.

with

$$\vec{k}_n \cdot \vec{r} = \mu_0 k (z \cos \bar{\theta} + x \sin \bar{\theta}) + nk^* x$$

and ξ_n describing the variation in amplitude of the light beam across the sound beam.

Thus, with the small change in refractive index due to the sound beam ($\mu' \approx 10^{-5}$), and assuming a solution of the form given in equation (6), it follows that:

$$\begin{aligned} \mu^2(x, t) &= \mu_0^2 + 2\mu_0 \mu' \\ &= \mu_0^2 + i\mu_0 \sum_{j=1}^{\infty} \mu_j \left\{ \exp[i(j\omega^* t - k^* x) + \delta_j] \right. \\ &\quad \left. - \exp[-i(j\omega^* t - k^* x) + \delta_j] \right\}, \end{aligned}$$

and the wave equation becomes:

$$\begin{aligned} \frac{\partial^2 \xi_n}{\partial z^2} - [2i\mu_0 k \cos \bar{\theta}] \left[\frac{\partial \xi_n}{\partial z} \right] - [(nk^* + \mu_0 k \sin \bar{\theta})^2 + (\mu_0 k \cos \bar{\theta})^2] \xi_n \\ = -\mu_0^2 k^2 \xi_n + i\mu_0 k^2 \sum_{j=1}^{\infty} \left\{ \mu_j [\xi_{n-j} \exp[i(j\omega^* t + \delta_k)] \right. \\ \left. - \xi_{n+j} \exp[-i(j\omega^* t + \delta_j)]] \right\}. \end{aligned} \quad (7)$$

In order to arrive at the required solution, it must be assumed that ξ_n is a slowly varying function of z , and with $\frac{k^*}{k} \ll 1$:

$$\frac{\partial^2 \xi_n}{\partial z^2} \ll \mu_0 k \frac{\partial \xi_n}{\partial z}.$$

Thus for progressive sound waves propagating at normal incidence to the light beam and with the time variation of ξ_n determined by the ω^* of the sound beam:

$$\xi_n(x, t) = \phi_n(z) \exp(in\omega^*t) \quad ,$$

and if there is only a $j = 1$ term in equation (3), equation (7) becomes:

$$\frac{d\phi_n}{dz} + \frac{\nu}{2L} [\phi_{n-1} - \phi_{n+1}] = \left(\frac{in^2 Q}{2L} \right) \phi_n \quad ,$$

with

$$Q = \frac{k^{*2} L}{\mu_0 k} \quad , \quad \nu_1 = \nu = k\mu_1 L \quad . \quad (8)$$

Therefore, equation (6) becomes:

$$E = \sum_{n=-\infty}^{\infty} \phi_n(z) \exp\{i(\omega + n\omega^*)t - \vec{k}_n \cdot \vec{r}\} \quad . \quad (9)$$

This represents a system of plane waves with wave vectors k_n , time independent amplitudes ϕ_n , and angular frequencies $(\omega + n\omega^*)$. The index n refers to the n th Fraunhofer diffraction order.

The Parameter Q

The solution to equation (8) depends on the parameter Q , with the quantities that determine Q normally fixed throughout the course of an experiment. However, since Q has a quadratic dependence on frequency its value can extend over 4 to 5 orders of magnitude. Over this great range the diffraction phenomenon goes through various stages. Thus, it becomes necessary to address the problem for three different cases: $Q \ll 1$, $Q = 1$, and $Q \gg 1$ (Klein and Cook, 1967). This investigation

is only concerned with the region consistent with making quantitative measurements--the case when $Q \ll 1$, or the Raman-Nath region. Only brief mention will be made of the other two regions.

Thus for $Q \ll 1$ (for a 2 Mhz sound beam $Q = 0.025$), equation (8) becomes:

$$\frac{d\phi_n}{dz} + \frac{v}{2L} [\phi_{n-1} - \phi_{n+1}] = 0 \quad (10)$$

Using the identity

$$\frac{dJ_{-n}(x)}{dx} = -\frac{1}{2} \left[J_{-(n-1)}(x) - J_{-(n+1)}(x) \right],$$

and the following boundary conditions

$$\xi_0(0, t) = 1, \quad \xi_n(0, t) = 0 \quad \text{if } n \neq 0$$

gives the solution to equation (10) at $z = L$ in the form:

$$\phi_n = J_{-n}(v) \quad .$$

Here $J_{-n}(v)$ is the n th order Bessel function of the first kind.

The intensity of the n th diffraction order is then given by:

$$I_n = (\phi_n)^2 \quad .$$

The parameter v is known as the Raman-Nath parameter and is a measure of the degree of phase modulation produced by the sound beam. This phase modulation can be determined by investigating the dependence of E , at $Z = L$, on the phase variable $(\omega^* t - k^* x)$.

Equation (9) can be written in the form:

$$E = \sum_{n=-\infty}^{\infty} J_{-n}(v) \exp(in[\omega^* t - k^* x]) \exp[i(\omega t - \mu_0 k L)] \quad ,$$

then:

$$\tan \Omega = \frac{\sum_{n=-\infty}^{\infty} J_{-n}(v) \sin n(\omega^* t - k^* x)}{\sum_{n=-\infty}^{\infty} J_{-n}(v) \cos n(\omega^* t - k^* x)} \quad (11)$$

Using the identities

$$\sin(z \sin \alpha) = 2 \sum_{k=0}^{\infty} J_{2k+1}(z) \sin\{(2k+1)\alpha\}$$

$$\cos(z \sin \alpha) = J_0(z) + 2 \sum_{k=1}^{\infty} J_{2k}(z) \cos(2k\alpha) \quad ,$$

equation (11) becomes:

$$\tan \Omega = \sin[v \sin(\omega^* t - k^* x)]$$

$$\cos[v \sin(\omega^* t - k^* x)]$$

then

$$\Omega = v \sin(\omega^* t - k^* x) \quad .$$

Thus, the light is modulated in phase with the light intensities for several diffraction orders shown in Figure 4.

The main features of the light diffraction theory are (Klein and Cook):

1. Many diffraction orders are observed and are a function of the Raman-Nath parameter v
2. At normal incidence the diffraction orders are symmetric,
 $I_n = I_{-n}$
3. The angular dependence is such that the maximum diffraction will occur at normal incidence
4. The light intensities in the n th positive and negative orders vanish together as v is changed

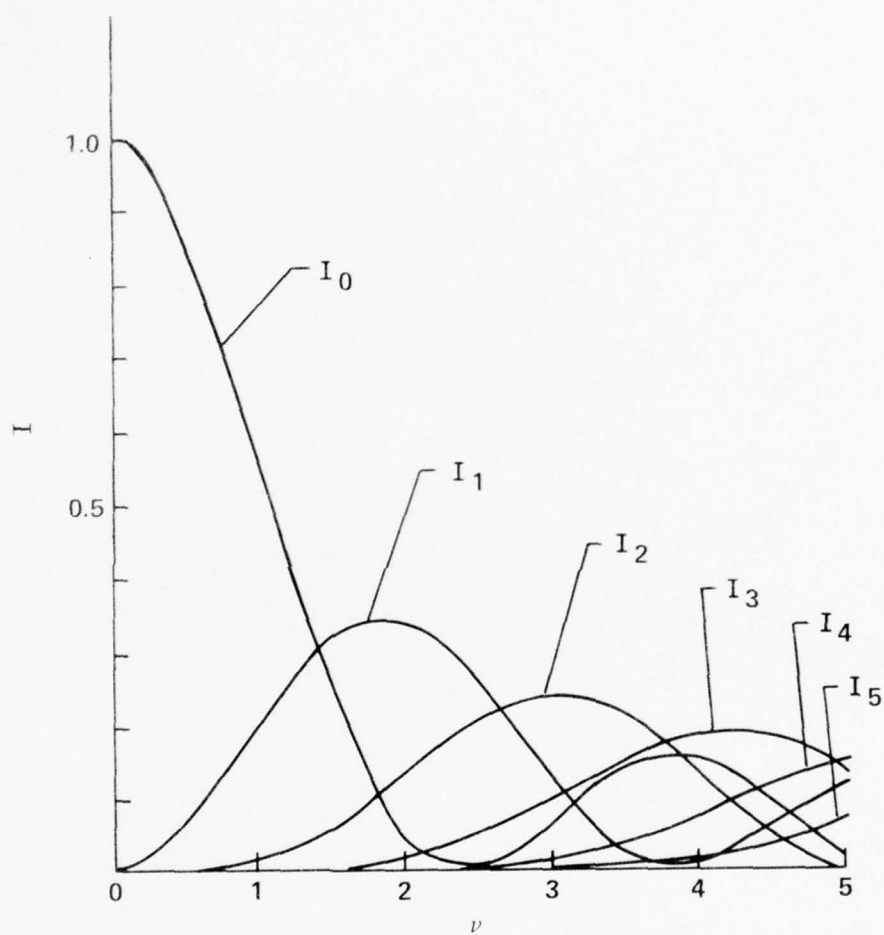


Figure 4. Light intensities of several Fraunhofer orders versus the variable v under Raman-Nath conditions.

5. The intensity will be symmetric around normal incidence
6. All of the above is only valid as long as the width of the sound beam is small compared to the width of the light beam.

As Q increases there is no longer a simple solution to the differential equations. Therefore the diffraction phenomenon can no longer be described purely by a phase modulation. As $Q \rightarrow 10$, the diffraction effect at normal incidence completely disappears. This is an area where Bragg diffraction is dominant. The orders are no longer symmetric and the majority of light appears in the zeroth and first orders.

The Variable v (the Raman-Nath Parameter)

The variation of refractive index produced by a sound beam is related to the sound pressure by the Ekman equation:

$$\mu = \frac{(\mu_0 - 1)(\mu_0^2 + 1.4 \mu_0 + 0.4)}{\mu_0^2 + 0.8 \mu_0 + 1} P$$

Since

$$v = k\mu L$$

for water the relation becomes:

$$P = \frac{v\lambda}{L} 10^9$$

or

$$v = \frac{P\lambda}{L} 10^{-9}$$

In order for the diffraction effect to be described by phase modulation, the Raman-Nath parameter must fall in the interval $0 < v < 2.4$ (Smirnov et al., 1973).

In Schlieren visualization the intensity of the image is a result of the interference of all the diffraction spectra produced by the sound diffracted light. This can be expressed as:

$$I = \sum_n \phi_n^2 \quad .$$

However, in Schlieren visualization a spatial filter is placed on the glass plate S2 (Figure 1) and effectively blocks out the zeroth order. The intensity is then given by:

$$I = 1 - \phi_0^2(r) = \sum_n \phi_n^2 \quad n \neq 0 \quad .$$

The light intensity is now expressed as a nonlinear function of the Raman-Nath parameter and it is only in the region where $0 < v < 2.4$ that a single valued relationship between the two quantities exists. A typical curve is shown in Figure 5.

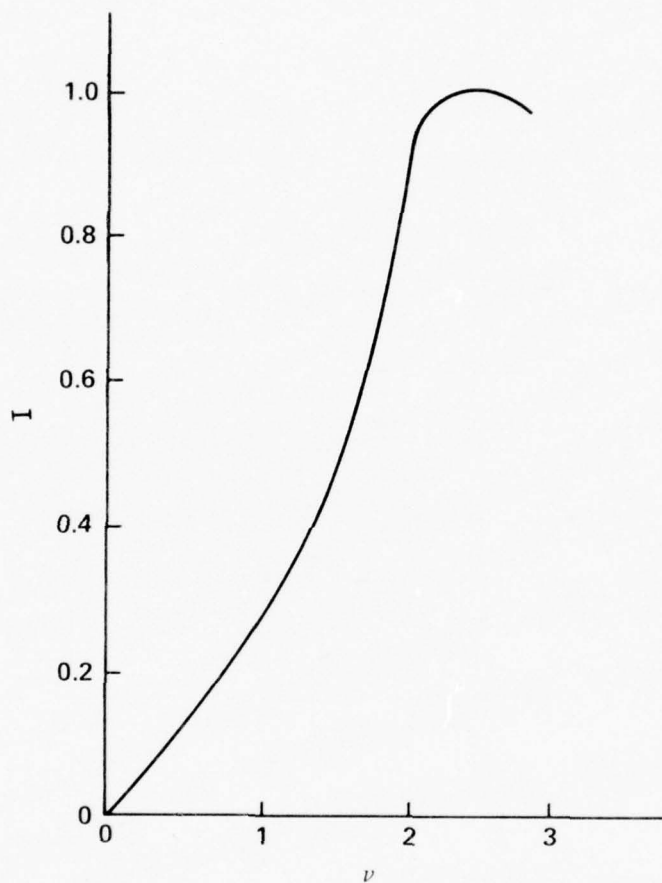


Figure 5. Image intensity as a function of the Raman-Nath parameter (Smirnov et al., 1973, p. 160).

III. ELECTRONICS

Imaging System

In order to develop a fast and reliable Schlieren system some type of imaging and data sampling method had to be selected. From past efforts it was clear that although photographic film was usable, it had limitations because of the special care needed in the photography and developing processes, and thus did not lend itself to the primary objective of this investigation.

Other methods considered were the photocell and the flying spot scanner, but again they did not appear to be suited to this study.

It was finally decided that the appropriate imaging device would be a closed circuit television camera (CCTV). With its assorted electronics, such an imaging device would best meet the needs of this investigation. Some of its obvious advantages are:

1. Inexpensive, easily available
2. Compact
3. High sensitivity
4. Wide range of associated electronics
5. Timed format of the output signal.

A discussion of the aspects of the CCTV camera and its composite output signal follows.

Vidicon Tube

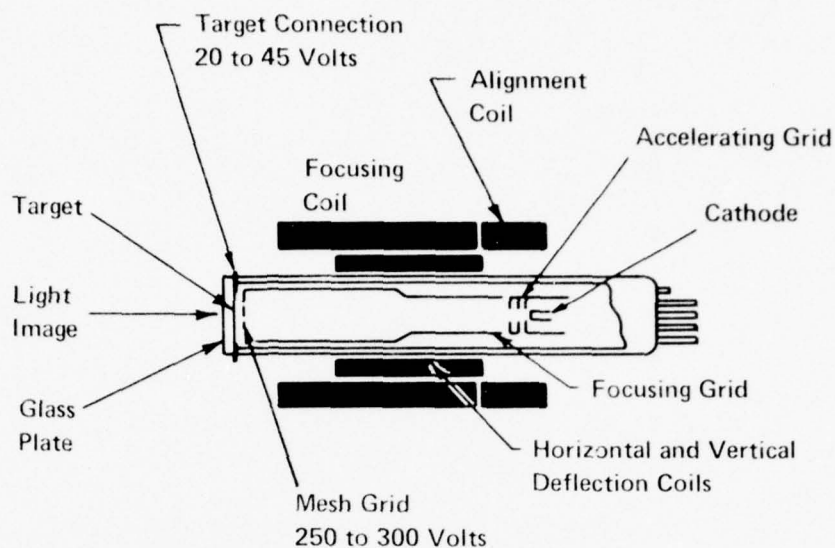
The primary component of a closed circuit television camera is a light-sensitive receiver and imaging device called a Vidicon tube.

The Vidicon tube, shown in Figure 6, is relatively simple and consists primarily of a photosensitive target plate and an electron gun. An optical image is focused on the target plate producing a charge image which is scanned by the electron beam.

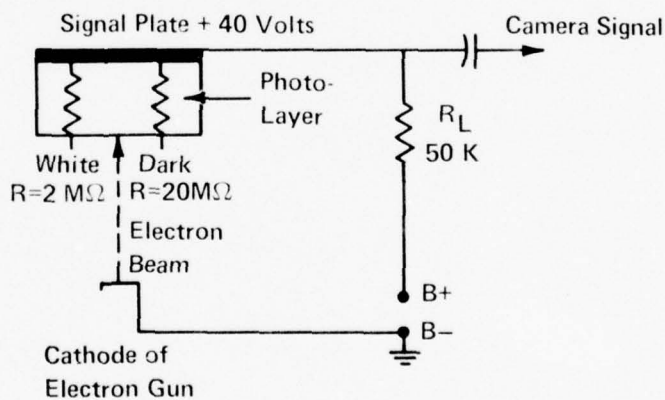
The target plate consists of two different layers: (1) transparent film of conducting material coated on the inside surface of a glass face plate which serves as the signal output connection for the camera; and (2) a thin coating of photoconductive material, generally selenium or antimony, on which the charge image is formed.

The photoconducting layer is a thin insulator. The image side had a dark current resistance of 20 megohms and is at a potential of 40 volts with respect to the cathode. Thus, the potential at each point on the gun side of the photolayer depends on the target's resistance to the signal plate voltage. Since the resistance of the photoconductive surface decreases with the amount of light, white light produces areas of low resistance and potentials close to 40 volts; dark areas have a high resistance and a lower potential. The result is a pattern of positive potentials on the gun side corresponding to the optical image seen by the target. This charge image is then scanned by the electron beam.

The primary components of the electron gun are a heated cathode, an accelerating grid, and a focusing grid. Deflection of the electron beam for scanning is produced by horizontal and vertical deflection coils in an external deflection yoke. A wire mesh grid is placed close to the target and held at a potential of several hundred volts. This



(a)



(b)

Figure 6. Vidicon camera tube. (a) Construction and operating voltages. (b) Signal circuit for camera signal output of Vidicon.

decelerates the electron beam so that electrons can be deposited on the charge image without producing secondary emissions.

When an image is focused on the target, each point on the gun side of the charge image is at a different positive potential. Electrons from the beam are deposited on the photolayer's surface, thereby reducing the positive potential towards the cathode voltage of zero. This change in potential causes a signal current to flow in the signal plate circuit and produces an output voltage across R_L (Figure 6b). For black areas the photolayer is less positive and the result is a smaller change in the signal current.

The universal scanning procedure employs horizontal linear scanning in an odd-line interlace pattern. In the United States, this pattern consists of 525 horizontal lines per frame repeated 30 times a second. The process is shown in Figure 7. Briefly, the electron gun starts its scan from position A and scans horizontally across the frame with a uniform velocity. At the end of a trace the beam returns rapidly to the left side of the frame and is ready to start the next horizontal scan. As the beam scans horizontally, it also undergoes a slight vertical deflection which is slow compared to the horizontal scanning rate. This allows many horizontal lines to be scanned during one cycle of vertical scanning.

The beam is now at the left edge and is ready to scan line 3, omitting line 2. In this way, 262-1/2 lines are scanned with the alternate lines left blank. The electron beam, at position B, returns to the top of the frame, position C, and scans the even lines in a

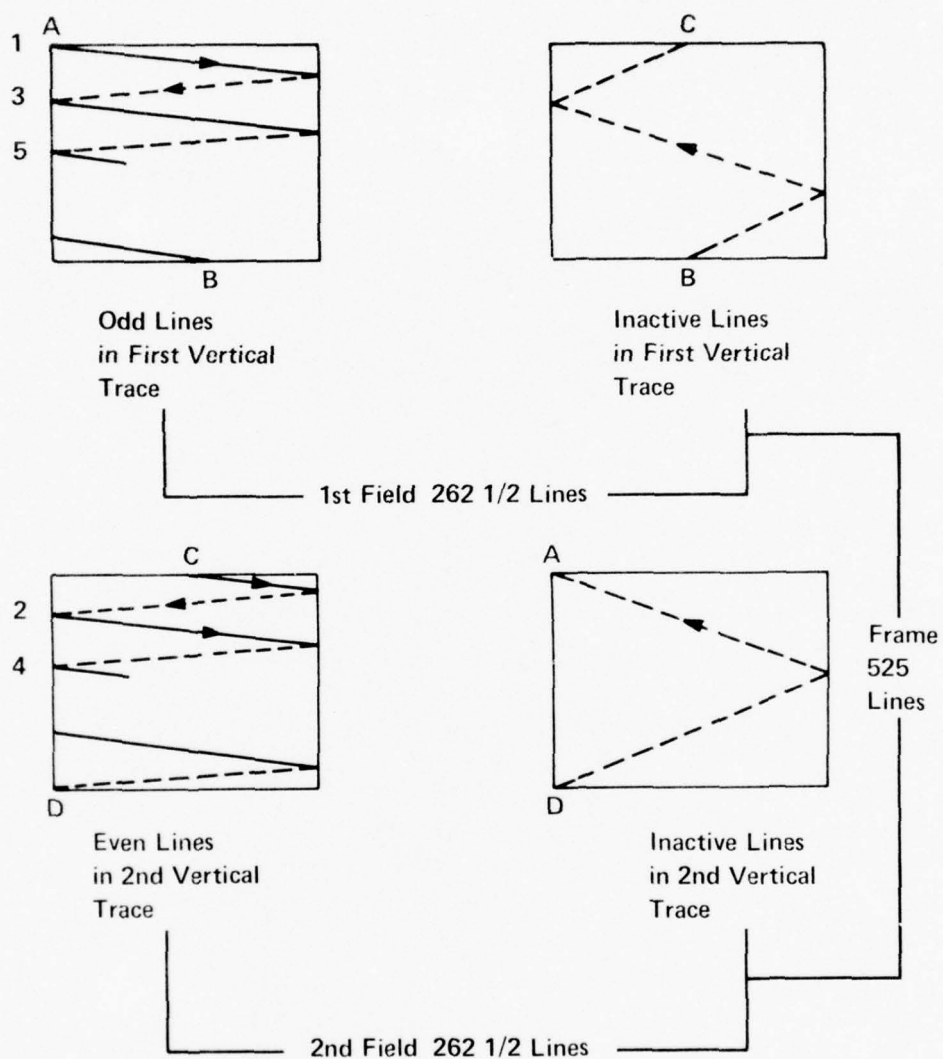


Figure 7. Odd-line interlaced scanning procedure.

similar manner, thus producing the 525 horizontal lines which make up one frame.

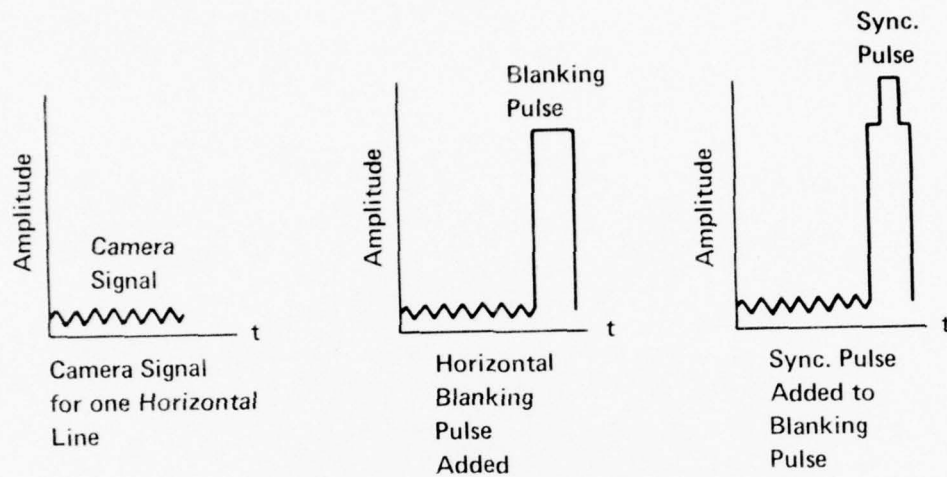
The horizontal scanning takes place at a frequency of 15.750 Hz and the vertical deflection frequency is 60 Hz. This gives a complete frame every 30th of a second.

The Composite Video Signal

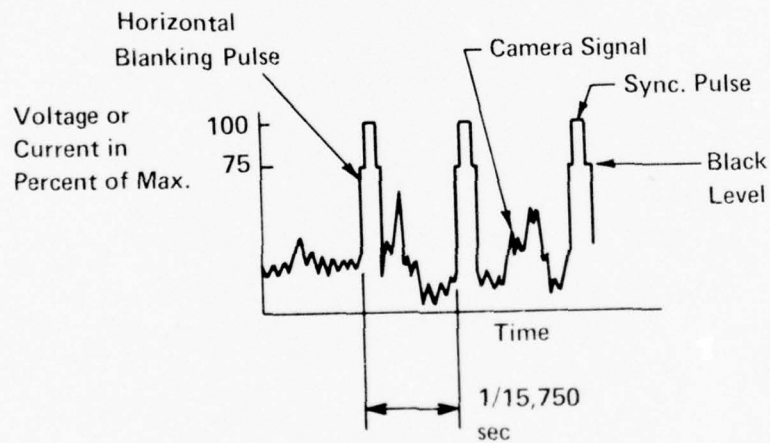
The composite video signal output from the CCTV camera is composed of the three parts shown in Figure 8. As the first line is scanned, camera signal variations are obtained with amplitudes corresponding to the required picture information. After the scan is completed and the beam is at the right side of the image, a blanking pulse is inserted to bring the video signal up to the black level so that the return trace can be blanked out. After the beam returns to the left side of the image, the blanking pulse is removed and the beam is ready to scan the next line. Also, a vertical blanking pulse inserted at the end of each vertical scan blanks out the signal during vertical retrace. Superimposed on top of each blanking pulse is an additional synchronization pulse. These pulses provide the signal for the electron beam flyback.

Analysis of the Composite Video Signal

The use of a CCTV camera necessitated a method which would enable the handling of a large volume of video information. Even the least expensive cameras can generate the equivalent of 60 million bits per second, a volume difficult to process even with today's sophisticated computer facilities. In addition, the 6 Mhz signal bandwidth posed a problem.



(a)



(b)

Figure 8. (a) The three components of a video signal. (b) Composite video signal for three consecutive horizontal lines.

One piece of equipment used in this investigation was a Biomation Model 802 Transient Recorder. This instrument is part of a new class of equipment which uses sophisticated digital techniques to record pre-selected sections of analog signals. The recorded signals are held in the unit's memory and can be reconstructed and displayed on an oscilloscope or plotted on an X-Y recorder. A basic circuit description is shown in Figure 9.

Since only a fixed number of points (1024) can be stored in the memory, the timing and control circuits determine the rate at which the analog signal is digitized. In effect, these circuits equally space the sample points over a preselected portion of the incoming signal. This transient recorder has sweep times ranging from 50 Hz to 2 Mhz and a bandwidth of 500 Khz. It was this low bandwidth that necessitated the development of a method to compress the high data rate of the video signal.

This compression was made possible by a new product developed at Teledyne Philbrick - a Model 4855 ultra-high speed sample-and-hold amplifier. This device has a 6 Mhz bandwidth with a 250 nsec acquisition time, thus making it ideal for high-speed signal sampling. The amplifier samples and holds the peak value of an input signal at the time it is triggered. When triggered again, the amplifier updates itself with the incoming signal and outputs the previously sampled peak value in the form of DC values ranging from 0 to ± 10 volts.

Although the transient recorder has its own internal time base clock, it is not suited to the sweep times of the television signal.

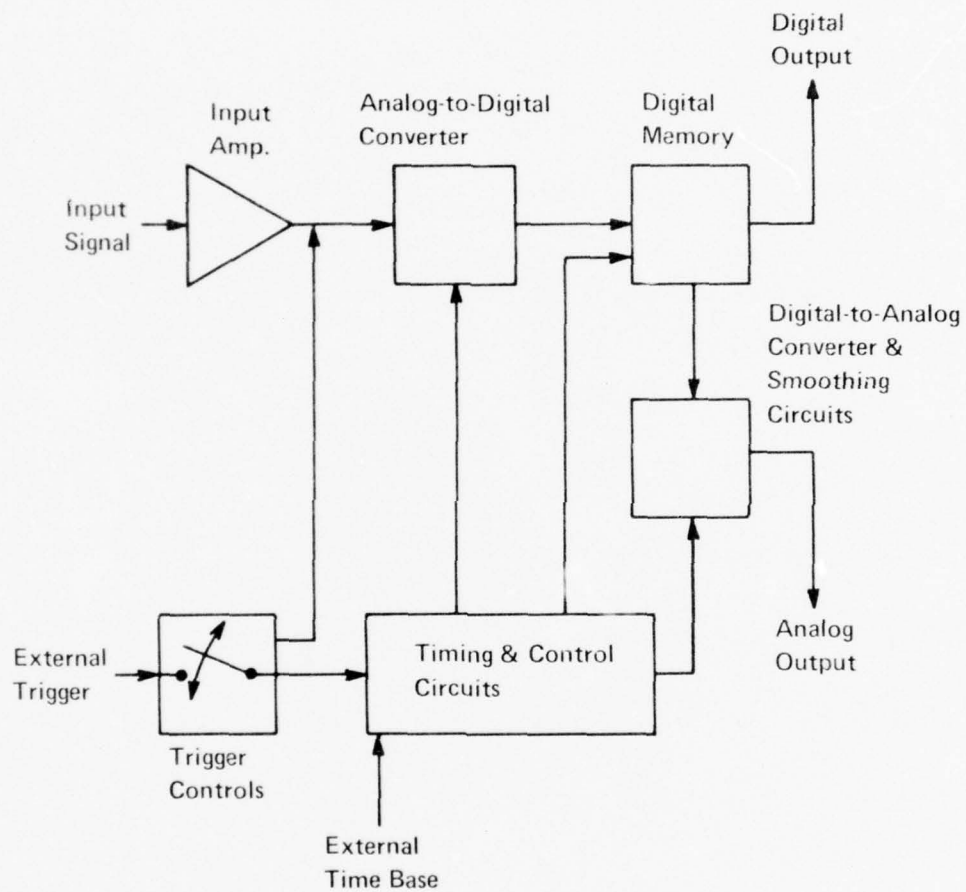


Figure 9. Circuit description of the transient recorder.

Thus, the internal clock was bypassed and an external pulse was used to digitize the incoming signal.

To compress the data rate of the video signal seen by the transient recorder, it was necessary to use the timed format of the television's blanking pulses. These pulses generated by the camera's internal crystal generator were used to trigger the sample-hold amplifier and served as the external time base for the transient recorder. In this way the signal going to the transient recorder had a frequency of 15.750 Hz, i.e., the horizontal scanning frequency.

However, in order to use the video blanking pulses, their format had to be altered. Both the transient recorder and the sample-hold amplifier require specific pulse forms. The developed Vidicon scan controller is shown in Figure 10.

The television camera's horizontal blanking pulses were fed into a pair of SN 74123 retriggerable, monostable multivibrators. Here the pulse width and rise time were set. By using a potentiometer, R1, it was possible to move this triggering pulse horizontally across the television raster. These pulses were then used to trigger the sample-hold amplifier and served as the time base for the transient recorder. Thus, the incoming video signal was sampled by the sample-hold amplifier at the horizontal scan frequency.

By this procedure, shown in Figure 11, a point was taken on each horizontal line. The first point was taken at position A on line 1, the second at point B on line 3, and so on. These values were each held by the sample-hold amplifier until it was triggered by the next horizontal pulse. The signal coming out of the sample-hold amplifier

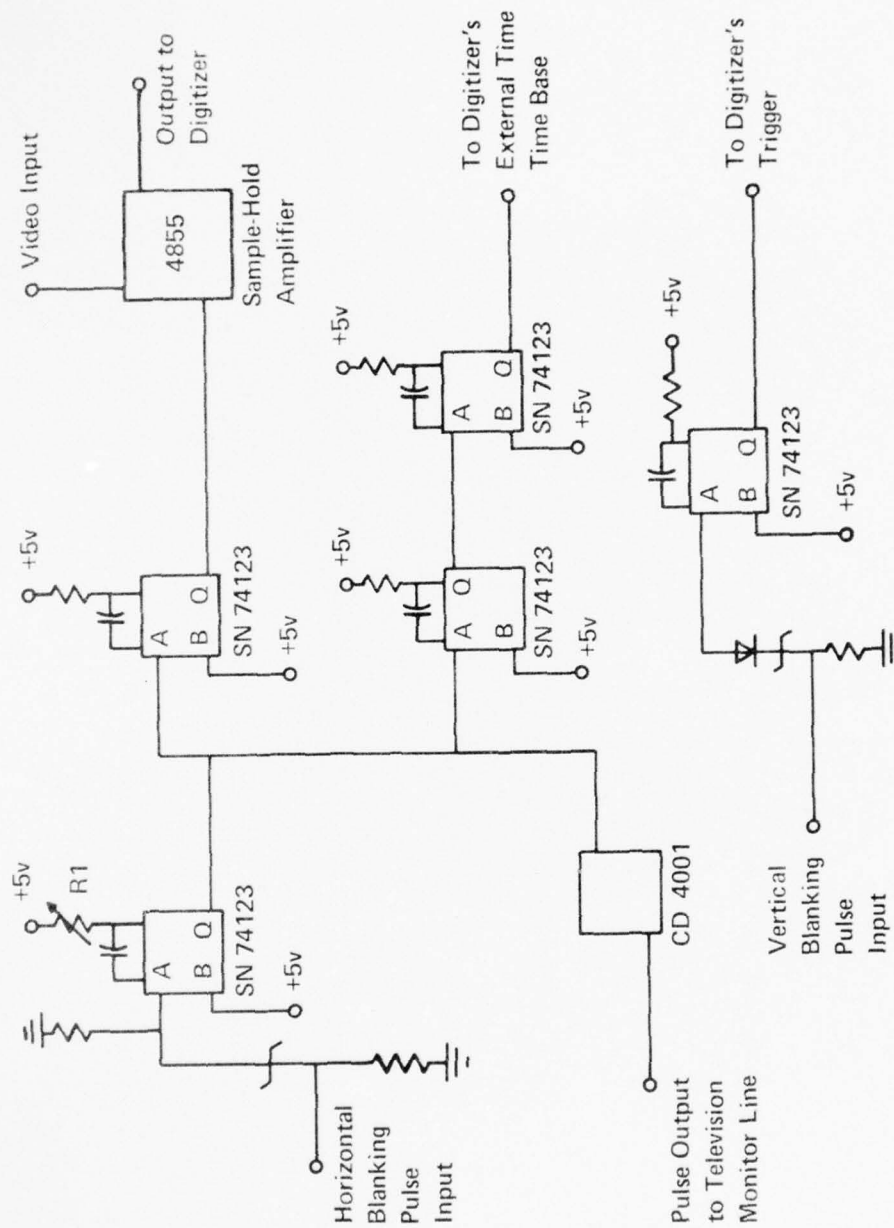


Figure 10. Vidicon scan controller

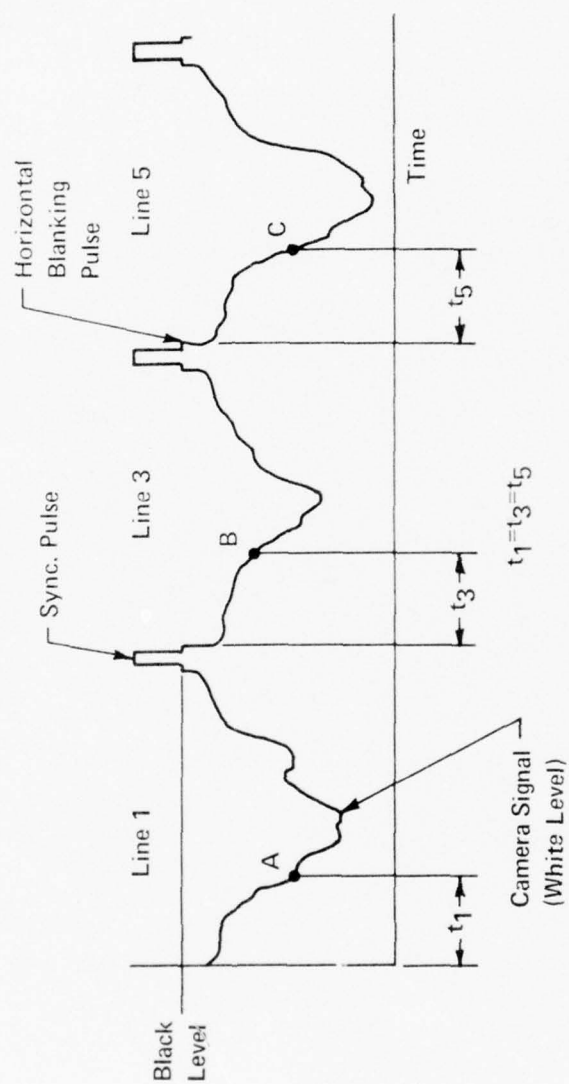


Figure 11. Sampling procedure.

was a video signal with a bandwidth of 15.750 Hz, i.e., it was a signal of video intensities in a vertical direction on the television raster. This output signal was fed into the transient recorder and digitized at the horizontal scan frequency.

The memory capacity of the transient recorder was 1024 bits of information. The method of operation was such that it would work until the memory was filled, then the digitizing would stop. The odd-interlace scanning of the television camera resulted in a sampling of the first, third, fifth, etc., lines, followed by a sampling of the odd-interlaced lines. In this way approximately four vertical video scans were placed in memory.

In addition, the horizontal blanking pulse was inputted to the video line through a CD 4001 integrated circuit. This placed a white vertical line on the television monitor at the position of the vertical raster scan. The vertical blanking pulse which occurs at the beginning of each series of horizontal scans, was fed into a SN 74123 and used to externally trigger the transient recorder and thus start the whole process.

There were several outputs available from the transient recorder. One was fed directly into an oscilloscope. With the transient recorder's controls set on auto and the trigger set on delayed sweep, a continuous display of the analog vertical intensity scan was thus available. A change in the delay, controlled by R1, moved the vertical intensity scan to a different position on the raster and an updated display appeared on the scope.

Another output was fed into an X-Y recorder. After the appropriate vertical intensity scan was located, the transient recorder's arm control was set to single, thereby holding in memory the intensity display presented on the scope. This analog signal was plotted on the X-Y recorder at the rate of 0.1 sec/word. A total time of 102.4 seconds was needed to plot the entire memory. A representative display is shown in Figure 12.

Therefore a method of effectively compressing the data rate of a CCTV camera's output video signal was devised and the electronics were constructed. It was through the use of this system that all the subsequent data on the Vidicon tube parameters and Schlieren intensity values were obtained.

Target Voltage

When marketing a commercial television camera, it is advantageous to incorporate an automatic sensitivity control circuit (ASC), into the camera's electronics. This circuit is used to maintain a constant video output over a large range of light intensities. However, this study was concerned with measuring video output voltages related to different scene intensities and therefore the ASC had to be bypassed. The ASC circuit initially in the camera is shown in Figure 13a. This circuit maintains a constant signal output by varying the voltage to the target through Q16. In the modified arrangement, Figure 13b, the output from Q16 was disconnected. In its place, a manual target voltage control was used. An 18 volt DC source was located on the camera's main circuit board and was connected to the target through R1. Thus, the Vidicon sensitivity and corresponding video signal output

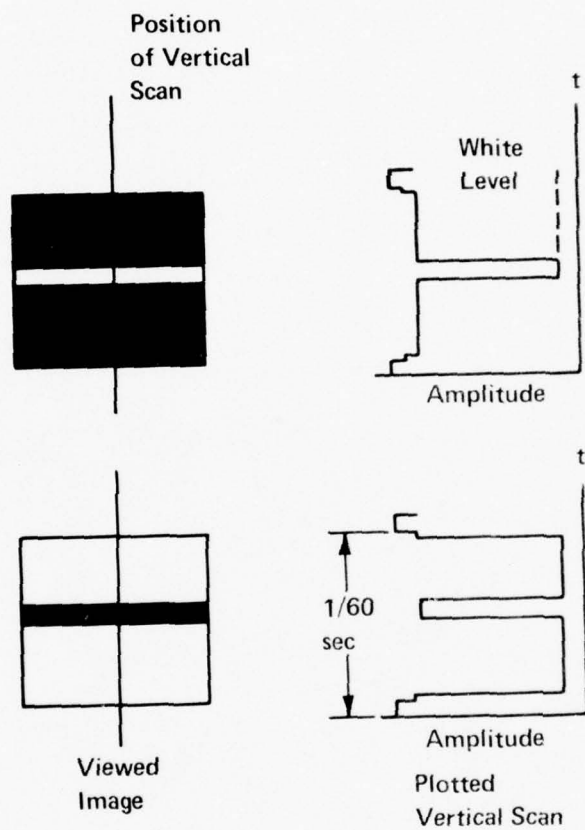


Figure 12. Representative vertical output.

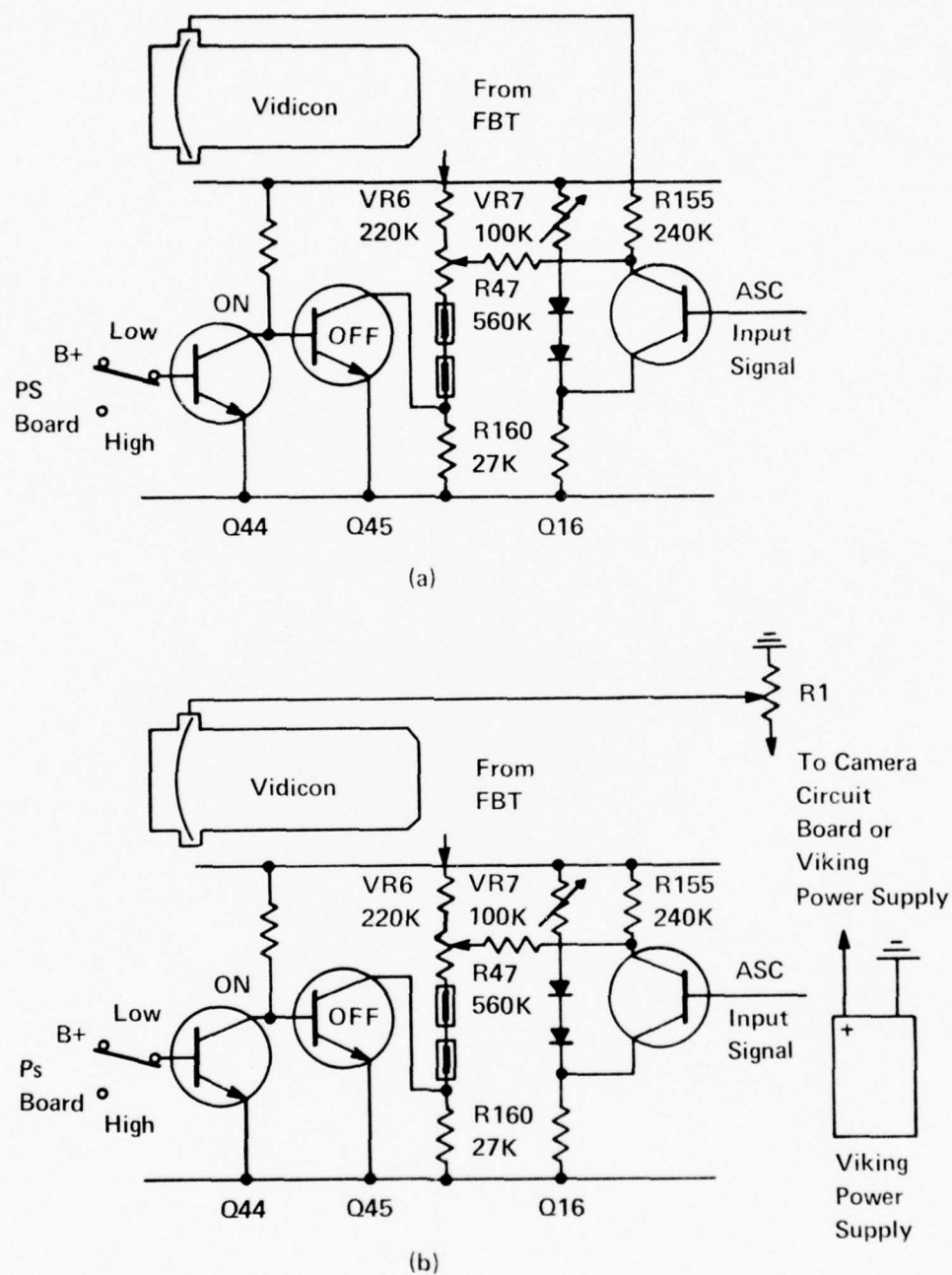


Figure 13. (a) Original Vidicon light sensitivity circuit.
(b) Modified light sensitivity circuit.

level could be manually controlled. This control was placed directly on the television monitor for easy adjustments.

However, the range of usable target voltages for the type of Vidicon tube used was from 10 to 35 volts. Thus, in order to obtain the increased sensitivity available from higher target voltages a 30-volt Viking DC power supply was used. Target voltages higher than 18 volts were used only at low light levels and then only for short viewing times, because the increased target voltage resulted in a dramatic increase in the dark current. In addition, high target voltages increased the possibility of burning the Vidicon's photosensitive layer.

Vidicon Tube Parameters

Before using the Vidicon tube to quantitatively evaluate an image, consideration had to be given to its performance characteristics and operating parameters. The most important for this investigation was the dynamic range, and to a lesser extent, the size resolution.

The dynamic range is a measure of the light intensity levels that can be detected without appreciable distortion. The dynamic range can also be related to another parameter, the gamma, which is defined as a measure of how much light intensities are expanded or compressed. For example, a gamma of one would mean that there is no change in the reproduced picture.

The size resolution is the image size above which the video signal output level does not change with a change in image size.

The television camera chosen for this investigation was a Sony AVC 3269. The Vidicon tube in this unit is a 2/3 inch separate mesh type 8844. This particular camera was chosen because it has an additional internal video amplifier that allows it to be used to view low light level scenes. The line resolution of this camera is 500 lines at the center and 400 lines at the corners. This was verified by using the standard test pattern shown in Figure 14. The size resolution curve shown in Figure 15 indicated that the smallest line that meets the size resolution condition is approximately 0.7 mm. This line produced a plot on the X-Y recorder that was about 1 mm wide. This is the smallest white line on the test pattern above which there is no signal amplitude change. However, this was only important when a small ray or caution in a Schlieren image was to be quantitatively analyzed.

A curve of the increase in dark current as a function of higher target voltages is shown in Figure 16. As can be seen from this curve, taken with the lens cover in place, the dark current noise increases at a rapid rate as higher target voltages are used.

The most important single parameter that describes the Vidicon tube's performance is the relationship between the scene intensity and the signal voltage output from the camera, referred to as the Vidicon tube's transfer characteristic curve. A series of these curves for the type 8844 Vidicon tube is shown in Figure 17. These curves were taken by using neutral density filters and recording the corresponding signal output voltages. An evaluation of the Vidicon tube's performance was therefore possible. From these curves it appears that the Vidicon tube has a dynamic range of about 80 levels of intensity. This is below the

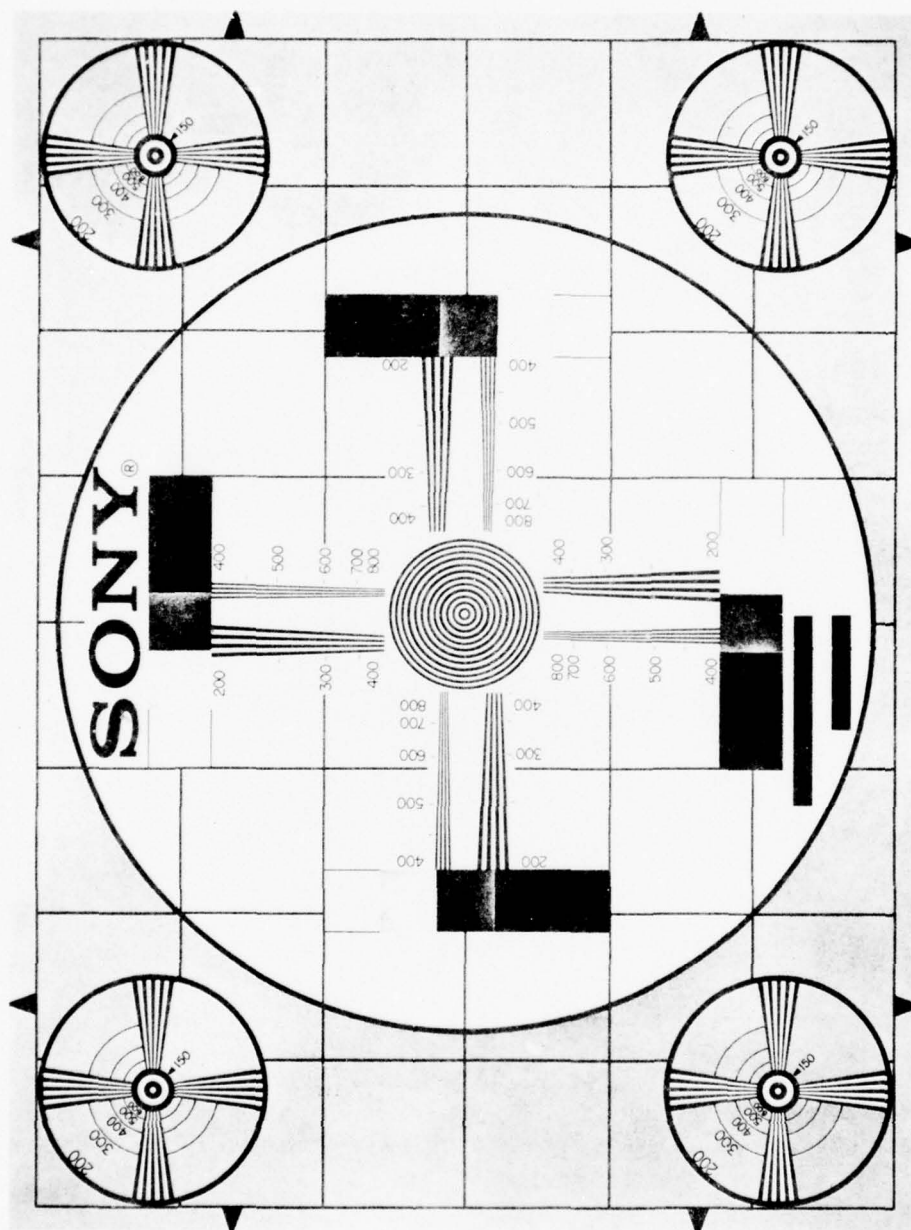


Figure 14. Standard test pattern.

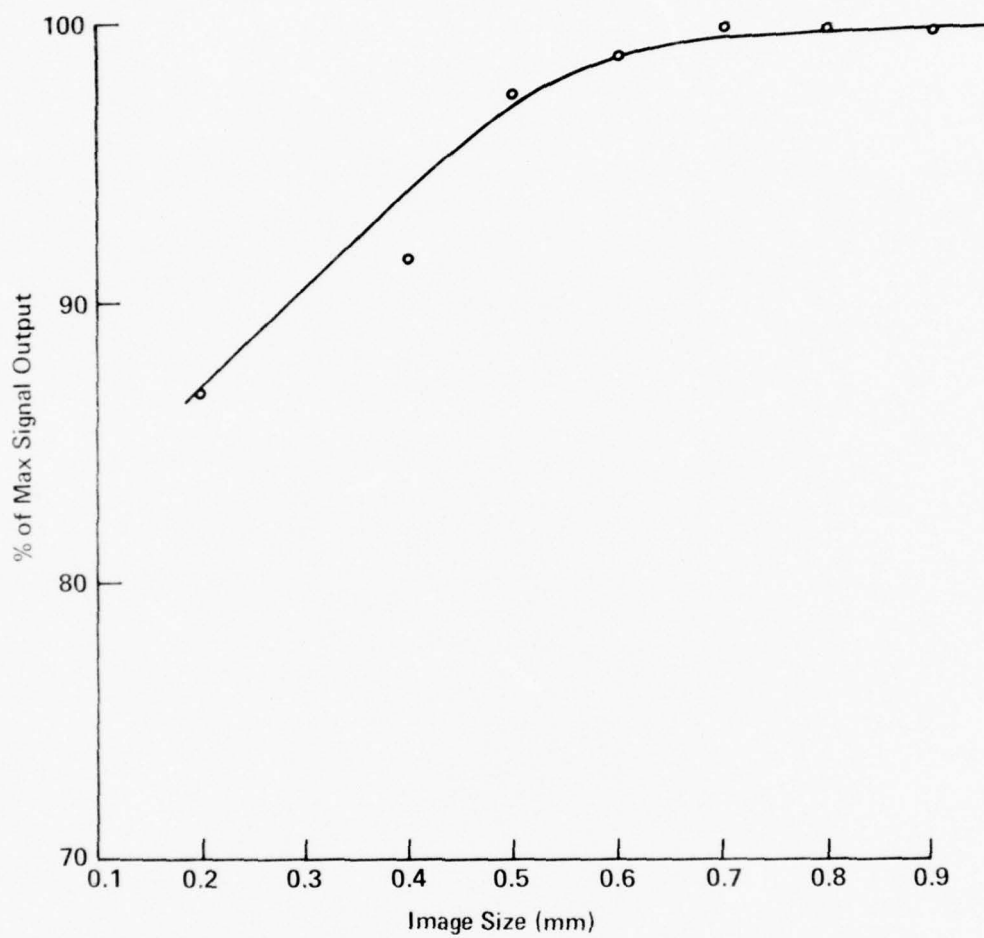


Figure 15. Image size resolution.

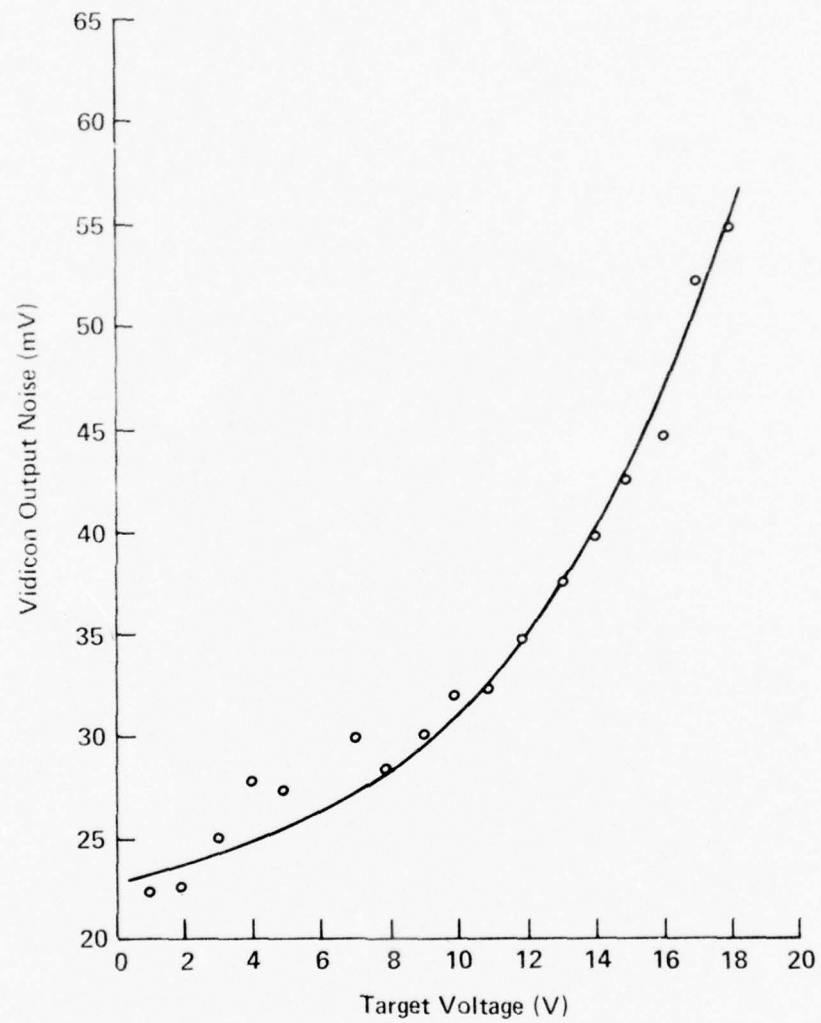


Figure 16. Vidicon dark current noise.

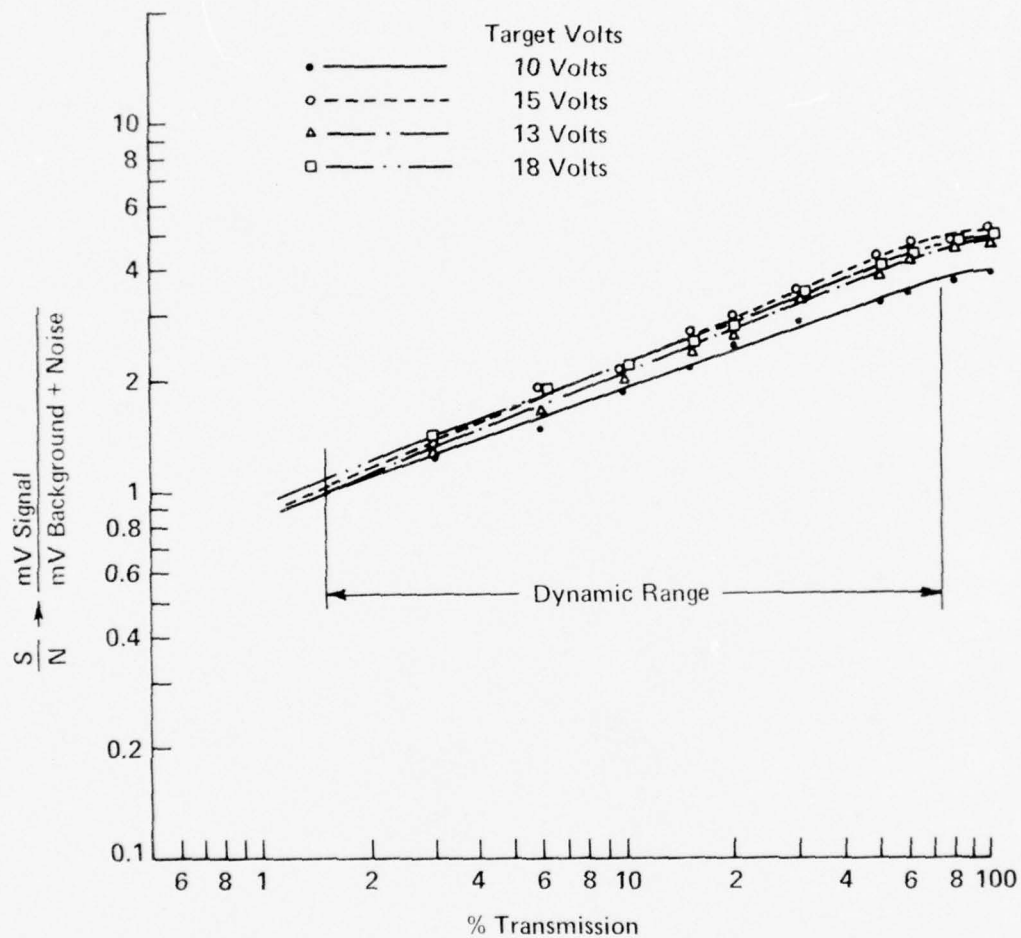


Figure 17. Vidicon transfer characteristic curves.

256 levels that can be digitized by the Biomation transient recorder. As expected, the signal-to-noise ratio for the 18-volt target voltage is lower because of the higher noise associated with higher target voltages. Further discussion of the format of the output signal and the method of analysis is given in Chapter V.

IV. THE SCHLIEREN SYSTEM

Schlieren Setup

A schematic of the Schlieren system setup is presented in Figure 18. The water tank was constructed of 3/4-inch thick lexan and measured 31 inches long, 20 inches wide, and 16 inches deep. Ten-inch holes were cut in three of the sides and plate glass windows installed. No attempt was made to obtain special glass as the standard 1/4-inch stock proved satisfactory. The side of the tank opposite the transducer installation was coated with simple molding clay. This clay proved to be a very effective sound absorbent and no reflections were observed from that side of the tank throughout the course of the investigation.

Initially the light source was a 100-watt mercury lamp, but as development proceeded the light source was changed to a General Radio Type 1538-A Electronic Strobotac. This instrument has a flashing rate ranging from 110 to 150,000 flashes per minute. The range used for this study had a flash duration of about 0.8 μ sec and an output intensity of one million beam candles. The strobe, although triggered by an internal oscillator, could also be triggered by an external one volt positive pulse. The light tube was xenon and was mounted in a 10° reflector. However, during the experimentation the reflector was removed because corrugations on the reflecting surface interfered with the final focusing of the light source. Instead, the xenon tube was mounted in a 2-inch diameter aluminum cylinder. The lenses L1 and L2 were coated achromats mounted in a similar 2-inch diameter aluminum tube, each with a focal length of 81 mm and a diameter of 45 mm. These lenses were used to focus the bright filament of the xenon tube onto the

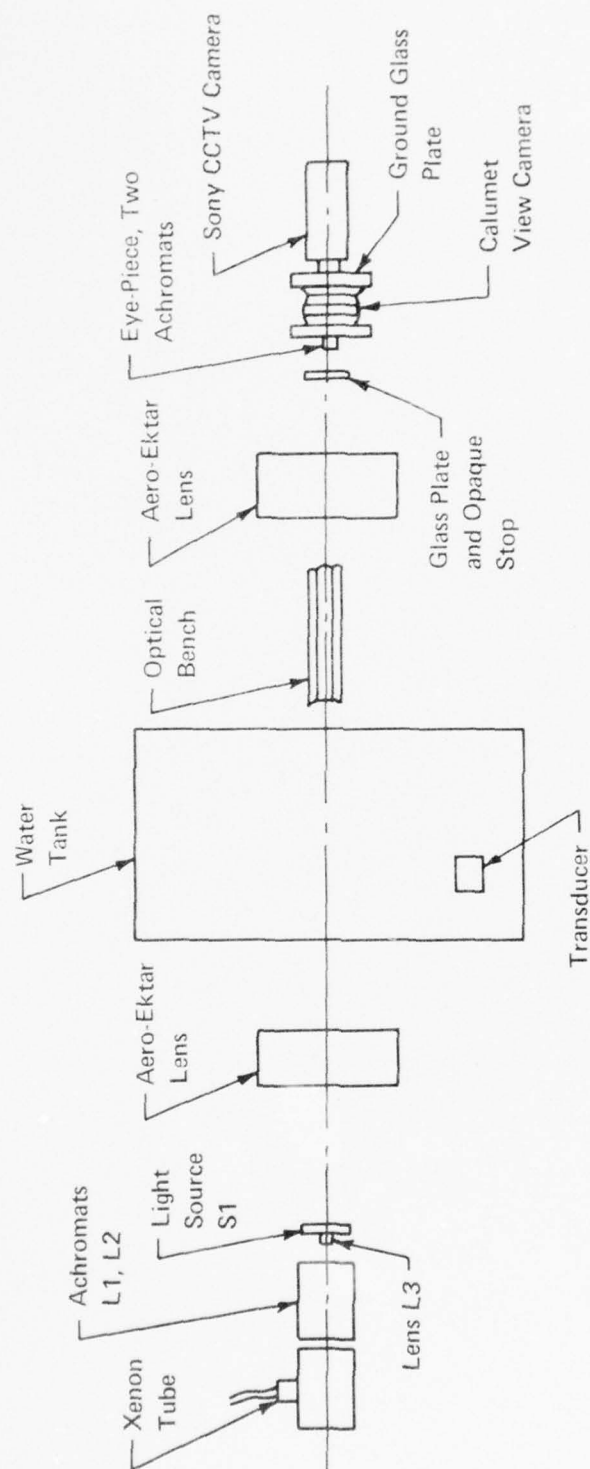


Figure 18. Schematic of Schlieren system.

adjustable slit or pinhole, S1. The openings of the slit ranged from several thousandths of an inch to 1/2 inch, and the pinhole diameters ranged from several thousandths to about 70 thousandths of an inch. Later in this chapter, the relative merits of a slit and a pinhole are discussed. It will be shown that there are only certain configurations when a slit proves to be acceptable for quantitative determinations.

The light from the slit, considered as the light source, was collimated by an Aero-Ektar lens with a focal length of 12 inches and a diameter of 309 mm. These lenses are used in high altitude photography and thus are color-corrected and of high quality. The xenon tube, the achromats, and the Aero-Ektar were adjusted for the brightest and most uniformly collimated light beam; the light beam was then passed through the windows of the water tank.

Although high-quality lenses were used, there was considerable difficulty in obtaining a light beam with a very uniform intensity over its cross section. But through experimentation, it was found that if a very short focal length lens, L3, was placed just before the slit, a collimated beam with a very uniform cross-sectional intensity resulted.

After passing through the windows of the water tank, the light beam was focused by a second Aero-Ektar onto a glass plate, S2. The second Aero-Ektar was similar to the first and the glass plate was placed at its second focal point. The image of the light source was thus focused on the glass plate. An opaque stop just big enough to block out the source image was situated on the plate, and therefore without a disturbance in the water tank, there could not be any light passing the glass plate. The light source, achromats, slit, Aero-Ektars,

and glass plate were mounted on a 4-meter Ealing precision optical bench, as shown in Figure 19.

It became evident during this research that lenses of the highest quality were a necessity for a properly functioning Schlieren system. The higher the lens quality, the sharper the source image and the sharper the separation of the diffraction orders.

Located behind the glass plate was a Calumet view camera with a removable Synchro-Comput shutter and a removable ground glass viewing screen. The camera was movable and was positioned to give the sharpest image of a sample situated in the water tank. A Polaroid film holder was placed in front of the ground glass viewing screen and Polaroid Type 51 high-contrast film was used to photograph the Schlieren image previously projected on the ground glass plate.

The Sony CCTV camera was mounted behind the Calumet view camera and its standard f1.8 lens focused on the Schlieren image. However it was soon discovered that due to the increasing angle of the light rays with distance from the center of the image seen on the ground glass plate, quantitative Schlieren measurements were questionable. Because of the long focal length lens needed to resolve the diffraction orders (discussed later in this chapter), the Schlieren image on the ground glass plate was large and rather dim. This was evident on the television monitor as only the central portion of the picture was of good viewing quality.

A method to overcome this difficulty was devised. The ground glass plate on which the Schlieren image is projected was removed and the television camera was focused on the aerial Schlieren image.

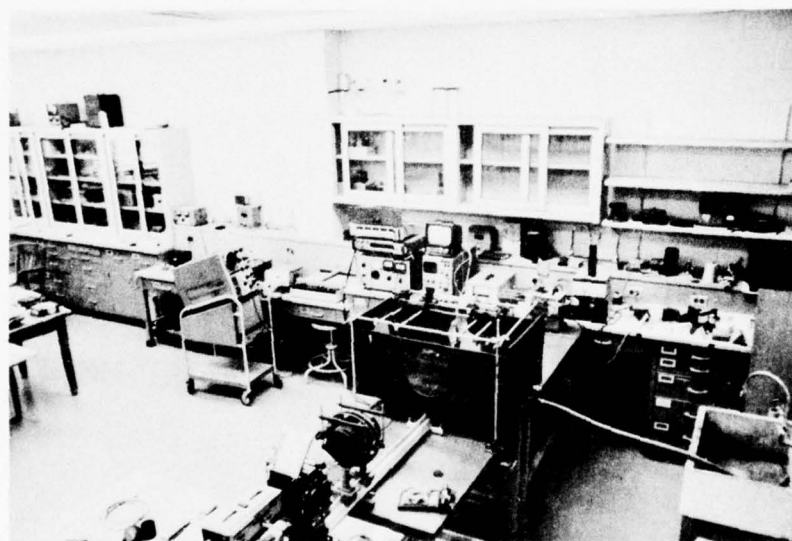
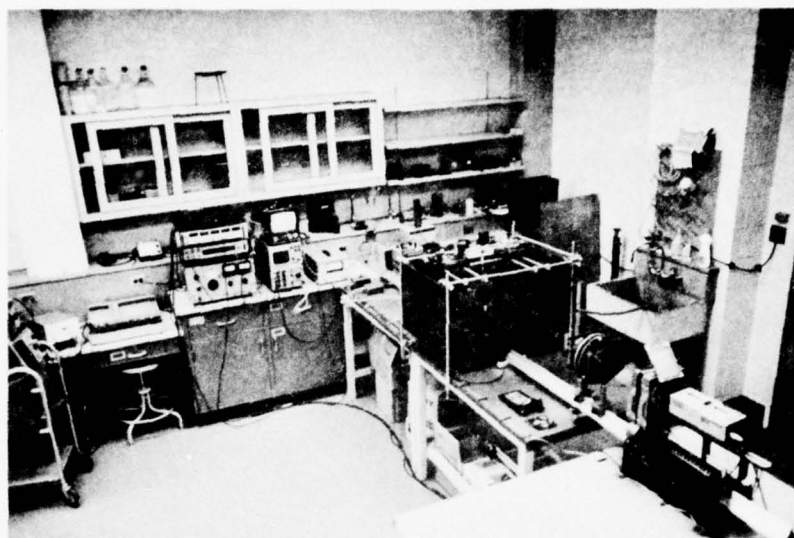


Figure 19. The Schlieren system.

However, in order to image the whole Schlieren picture onto the Vidicon tube, a series of auxiliary lenses had to be used. Two of these lenses were achromats with focal lengths of 80 mm. These achromats had a diameter of 40 mm and were mounted in an aluminum tube. The other lens was a telescope eyepiece with a focal length of about 25 mm. This lens was mounted in a piece of aluminum tubing that fit over the section containing the two achromats. The entire assembly was secured on the front of the 1.8 lens on the Sony camera. The camera was moved right up behind the glass plate with the opaque stop. Thus, all the light that formed the aerial Schlieren image was collected by the first lens and the light rays were progressively bent so as to focus the entire Schlieren image on the Vidicon tube.

The result was a marked increase in the intensity and uniformity of the Schlieren image seen on the monitor. Therefore meaningful quantitative measurements could be made. Using this arrangement it was possible to view the Schlieren image with the CCTV camera and then by moving the camera back to project the image on the ground glass plate of the Calumet view camera and photograph it.

The Schlieren system's optics, when properly aligned, were of such high quality and the light beam so highly collimated that the Schlieren image viewed by the CCTV camera did not suffer any intensity changes when the large overhead room lights were turned on.

Transducers

In this research there was no attempt to secure any of the commercially available transducer assemblies. Instead, simple devices were constructed using small discs of barium titanate and lead zirconium titanate. These discs had diameters ranging from 2.5 cm to 1.2 cm and thicknesses of 0.6 cm.

The discs were epoxied into lexan and copper holders. In all cases an air gap was left behind each disc as it was epoxied. It is believed that this resulted in a more uniform acoustic output and allowed more power to be radiated into the water (Breazeale and Adler, 1974). A motorized positioning device was constructed which enabled the transducer to vary its angle of incidence with respect to the sample.

Tradition dictates that the best way to deliver the maximum power to a crystal and thus into the water is to match the input impedance of the transducer to the output impedance of the driving amplifier. However, matching a transducer over a broad bandwidth is a difficult task. Instead of attempting to match transducer and amplifier, it was decided to use a new generation of power amplifiers recently made available. These solid state instruments developed by Electronic Navigation Industries (ENI) utilize the latest hybrid combining techniques to achieve the highest bandwidth and power output of any comparable amplifier. The great advantage ENI amplifiers have over conventional amplifiers is that although they all deliver maximum power into a 50-ohm load, ENI amplifiers deliver their maximum power rating into any load. The difference is that the power reflected due to a mismatch is absorbed

back into the amplifier. For example, a 10-watt conventional amplifier might deliver 2.5 watts into a 25-ohm load while a comparable ENI amplifier will deliver 9 watts into the same load and absorb one watt.

A Model 240-L ENI amplifier was selected as the power source for this investigation. This amplifier has a frequency response which covers 20 Khz to 10 Mhz and can supply 150 watts of C.W. and pulse power. This type of power amplifier makes it possible to drive the transducers at different frequencies without attention to matching requirements.

The input signal to the ENI power amplifier was supplied by a Dranetz series 206 digital tone burst generator. The series 206 uses the output of a Hewlett Packard Model 606-B AC signal generator as the triggering source to generate a single burst, a repetitive burst, or a continuous signal output. The length of each pulse can be varied from 10 μ sec to several seconds with periods ranging from 0.1 μ sec to 999.9 μ sec. Also a square wave output and a pulse output can be delayed with respect to the primary pulse. In this study the positive pulse was used to externally trigger the General Radio Strobotac for operation in the pulse mode. The instrument arrangement for the Schlieren system is shown in Figure 20.

Various Modes of Operation

There were two modes of operation used in this study: the continuous mode and the pulsed mode. In the continuous mode, the tone burst generator's controls were all set on their continuous settings and the strobe light set to work on its internal trigger. The result was the Schlieren image shown in Figure 21.

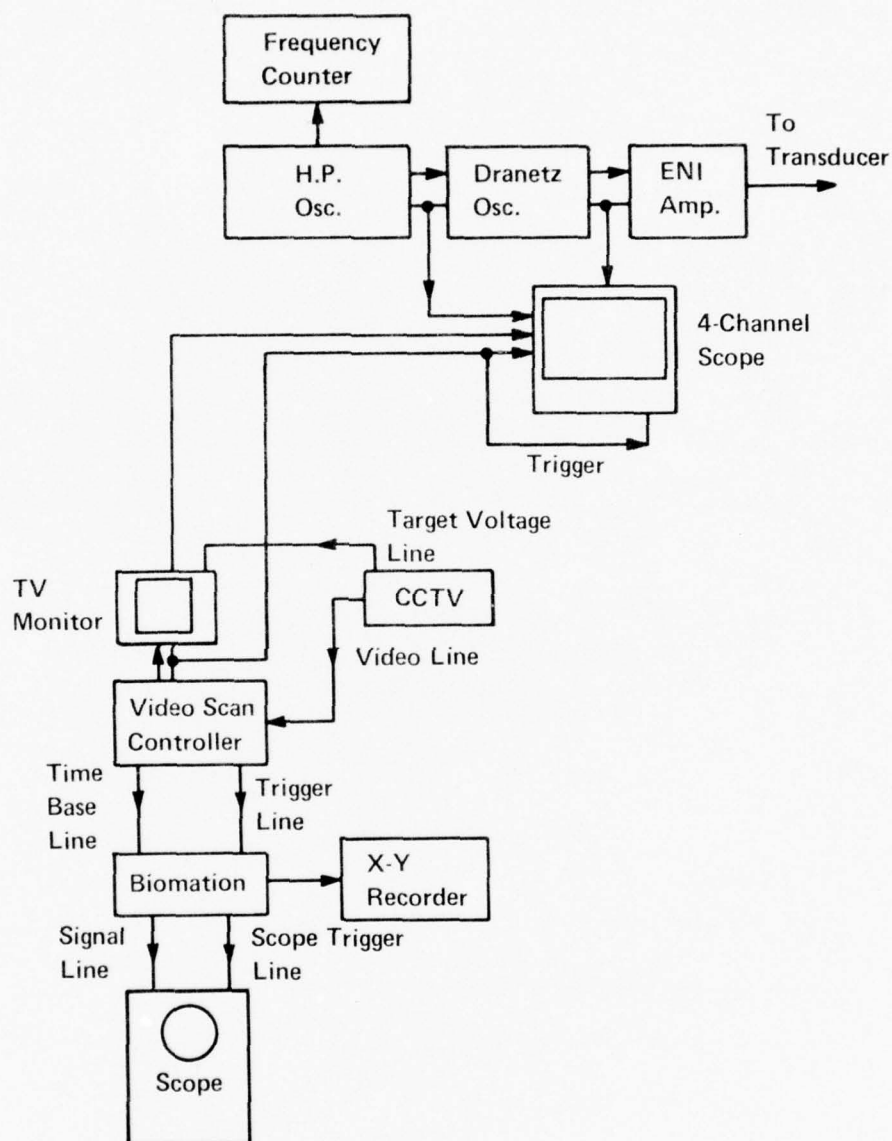


Figure 20. Instrument setup for Schlieren system.

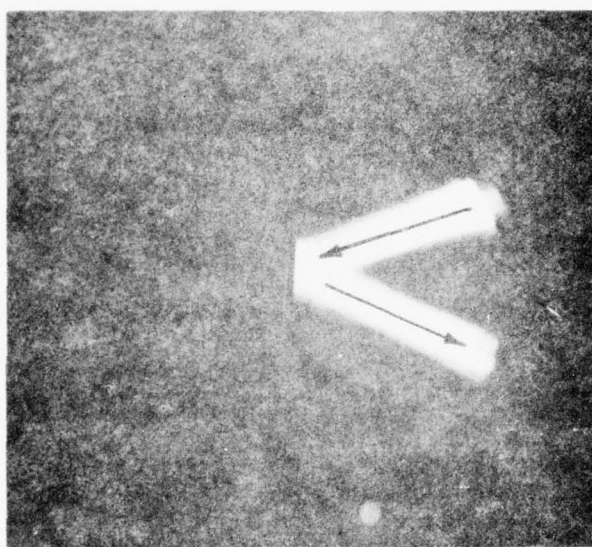


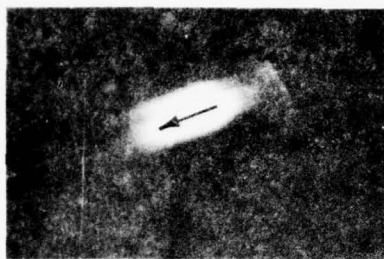
Figure 21. Continuous acoustic beam incident on a steel plate.
Frequency = 4.62 Mhz.

In the pulsed mode of operation the tone burst generator's controls were set on their pulsed settings and the auxiliary positive pulse was used to trigger the Strobotac. Using a short pulse output to the transducer and time delaying the positive pulse triggering the Strobotac, a single pulse of acoustic energy appeared in the Schlieren image. Varying the time delay then made the pulse move across the Schlieren image as shown in Figure 22. The pulsed mode of operation proved to be especially valuable since the use of short pulse lengths and the appropriate time delay allowed only the reflected and transmitted pulses to appear.

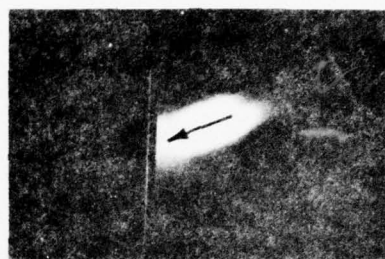
Format of the Output Signal

Figure 23 shows a continuous acoustic beam incident on a thin steel plate. The corresponding vertical intensity scan as it appears on the X-Y recorder is also shown. Proceeding from top to bottom on the intensity scan, the first peak is the vertical synchronization pulse and the flat plateau is the vertical blanking pulse. The next peaks are the intensities of the incident and reflected beams and at the bottom, the vertical synchronization pulse and blanking pulse are again present.

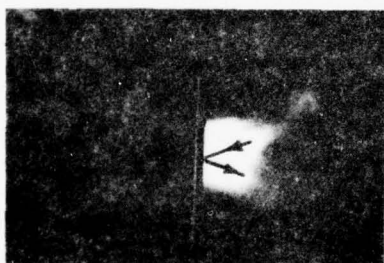
The line A-B represents the Vidicon's dark current noise at a particular target voltage when the cap is on the camera's lens. When power is not applied to the transducer and when the lens cap is removed from the camera's lens, the line C-D is a measure of the intensity of the background illumination. This background light is a result of some of the focused light from the source bypassing the opaque stop on the glass plate. If the lenses had been perfect, the background level would



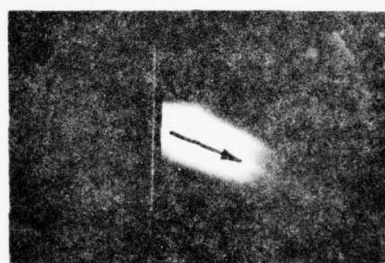
1



2

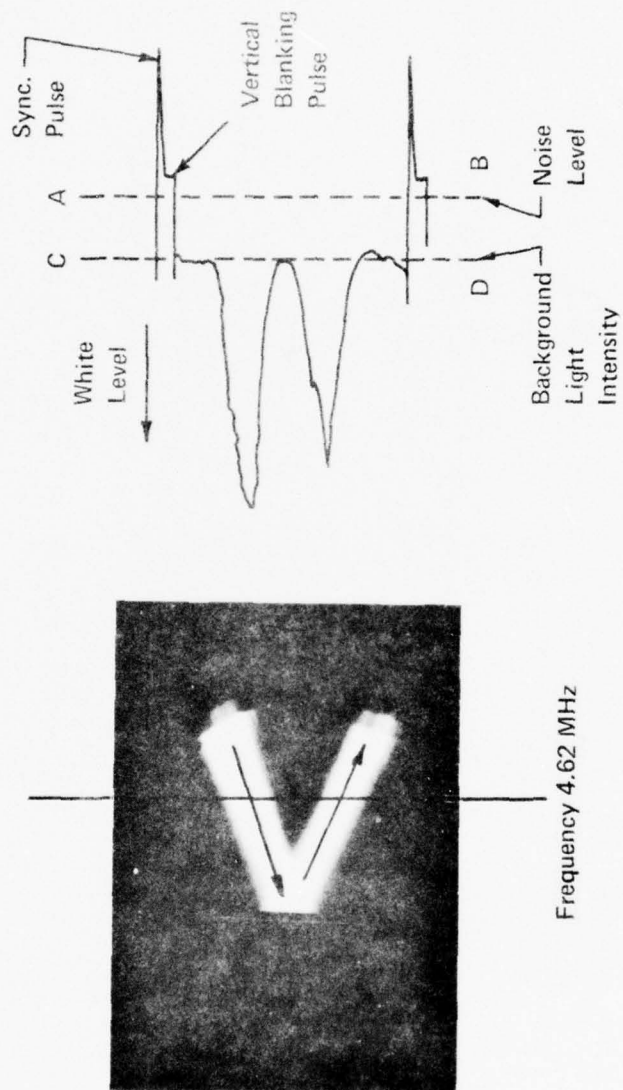


3



4

Figure 22. A 20- μ sec pulse incident on a steel plate. Frequency 4.62 Mhz. Each photo 10- μ sec later.



have remained at line A-B. As power was applied to the transducer, peaks representing the intensities of the incident and reflected acoustic beams became visible. For quantitative determinations, the intensity levels of the peaks were taken with the vertical blanking pulse as the zero level.

Critical Constants

As discussed in Chapter II, it was necessary to conduct the experiment within the range where only phase modulation of the light by the acoustic beam was present, i.e., the Raman-Nath region. The critical constants in the region of phase only modulation are:

$$Q = \frac{k^* L}{u_0 k} < 1 \quad \nu = ku_1 L \quad 0 < \nu < 2.4$$

The values of Q for the range of frequencies used and for all transducer configurations were in all cases below unity.

The Slit versus the Pinhole as the Light Source

In this investigation consideration was given to the type of light source used. In past studies on light diffraction, investigators have used both slits and pinholes, but they have not indicated how each affects the performance of their Schlieren systems.

In the initial arrangement of the Schlieren system, a pinhole was used as the light source. However, in order to attain the brightest image possible, the pinhole was replaced by a vertical slit. Slit openings as small as 0.004 inch resulted in very bright and high-quality Schlieren images, whereas pinholes with diameters as large as 0.016 inch did not produce Schlieren images of the same quality.

However, as the development continued, it was soon evident that for a Schlieren system to function correctly at all sound beam angles, a pinhole had to be used as the light source. The reason becomes clear if Figure 24a is examined. The diffraction orders produced because of the phase modulation of the light occur only in the direction of propagation of the acoustic beam. As the beam angle is changed from θ_1 to θ_2 , the positions of the diffraction orders are also changed. In this way, acoustic reflections and transmissions that occur at other angles are resolved from the opaque stop.

If a vertical slit is used as the light source and the sound beam is at 90° with respect to the vertical slit, the diffraction orders separate from the opaque stop in the usual manner. However, as the beam angle is changed to θ_2 , Figure 24b, the position of the diffraction orders also changes with the result that they are not all resolved from the opaque stop. Thus, light intensity losses occurring at angles other than 90° cannot be directly related to acoustic losses.

With the high quality of the Schlieren system's optics and with the extreme sensitivity of the Sony CCTV camera the lower light levels associated with a pinhole light source proved to be of little concern. Clear, bright, and uniform Schlieren images were present at all frequencies. In most cases the transducer voltage had to be lowered so as not to drive the Vidicon tube into saturation.

Low Frequency Limit

As the frequency of the acoustic beam was lowered, it became increasingly difficult to resolve the first diffraction order and the blocked out zeroth order. This was especially true when the slit was

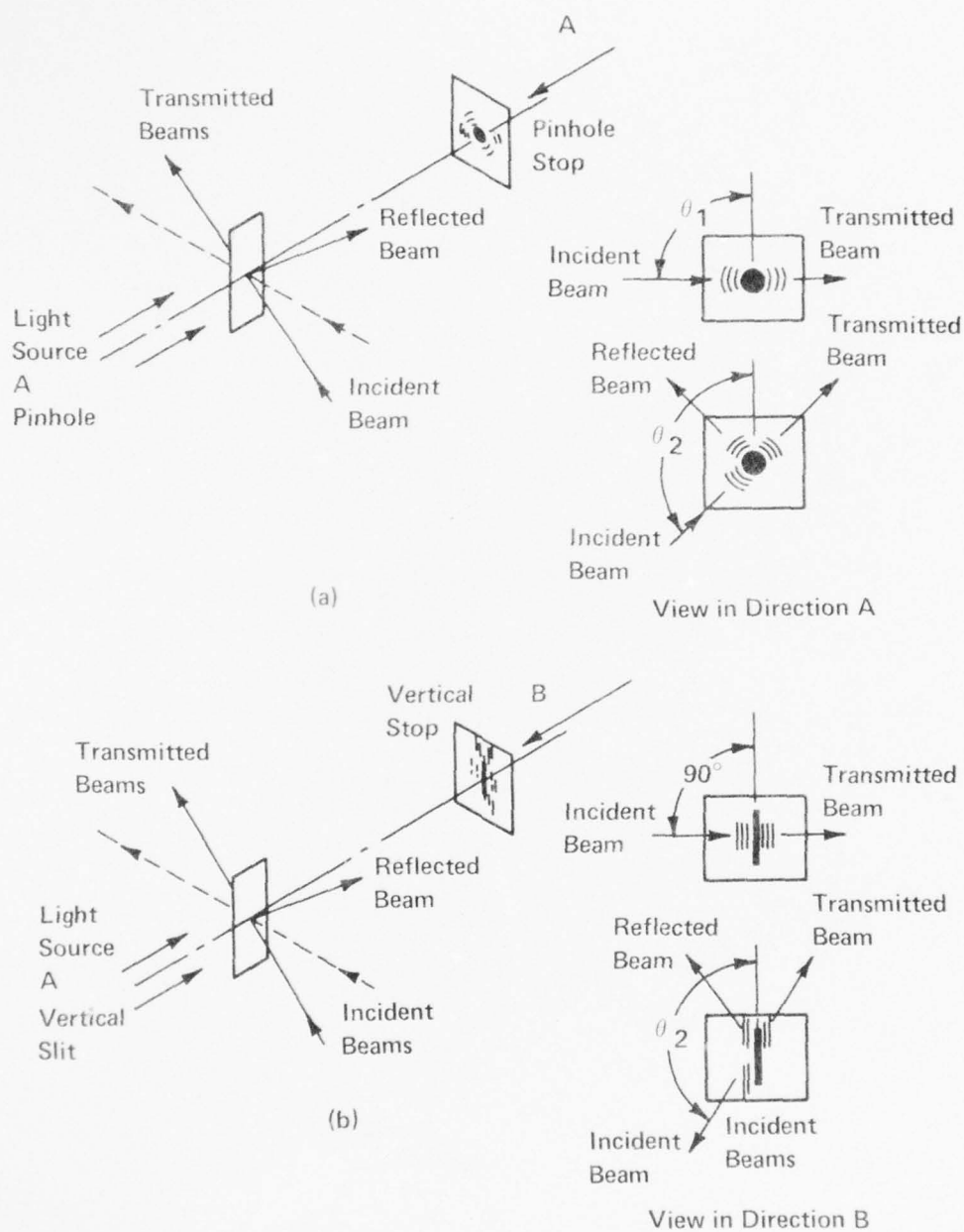


Figure 24. (a) Diffraction orders for a pinhole light source.
 (b) Diffraction orders for a vertical slit light source.

replaced by a pinhole. The larger diameter pinhole resulted in a larger stop on the glass plate S2. Thus at low frequencies the first diffraction order did not totally resolve itself from the opaque stop.

The conditions under which the diffraction orders are still resolvable are given by:

$$\sin \theta = \frac{n\lambda}{\lambda^*} \quad , \quad d_n = F\theta$$

where for small angles

$$\theta = \frac{n\lambda}{\lambda^*} \quad .$$

The distance between adjacent orders is now given by:

$$d_n = \frac{nF\lambda}{\lambda^*} \geq b$$

or

$$f \geq \frac{cb}{nF\lambda}$$

where b is the width of the stop.

Thus it follows that the use of a longer focal length lens would lower the working frequency of the Schlieren system. In this particular system with its high sensitivity, even if part of the first diffraction order was partially blocked out, quantitative measurements were still possible. The practical lower limit of the Schlieren system was about 300 KHz.

V. RESULTS AND DISCUSSION

Vidicon Surface Characteristics

In order to make quantitative Schlieren measurements using a closed circuit television camera, the variation in response across the Vidicon tube's photosensitive surface had to be evaluated. This was performed in the following manner: The opaque stop was removed from the glass plate, S2, thus illuminating the Vidicon tube with the full intensity and the entire cross section of the collimated light beam. A neutral density filter was placed in the system to set the light intensity level at a point midway in the tube's dynamic range. As illustrated in Figure 20, the video output signal to the television monitor was connected to one channel of the four-channel scope while the scope was externally triggered by the horizontal blanking pulses present in the video signal. Thus the horizontal scan lines were displayed over the full range of graduations appearing on the face of the scope (Figure 25). Vertical intensity scans were taken at the center of each of the eight horizontal squares shown in Figure 25, and were themselves divided into nine sections. This divided the Vidicon surface into a 72-square grid.

Figure 26 shows the result of taking the intensity at the center of each square and comparing it to the reference level, line A-B. The response horizontally across the Vidicon's photosensitive surface shows only slight variation. The only exception occurs near the Vidicon's sides. However, vertically there could be as much as a 10 to 15% drop in the Vidicon's response. Thus, when comparing intensity levels

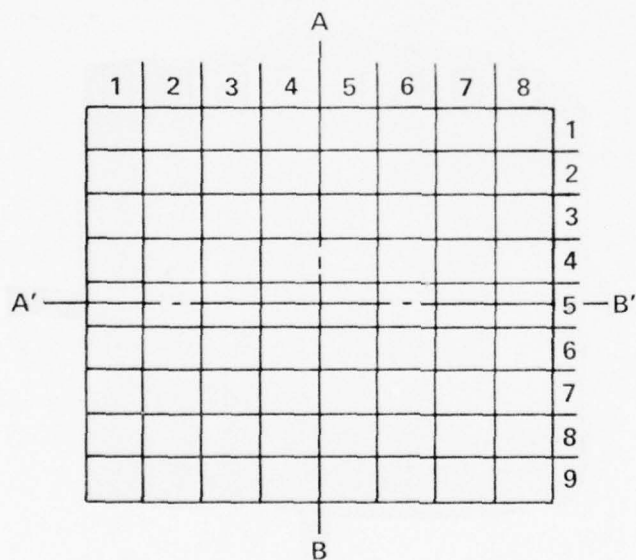
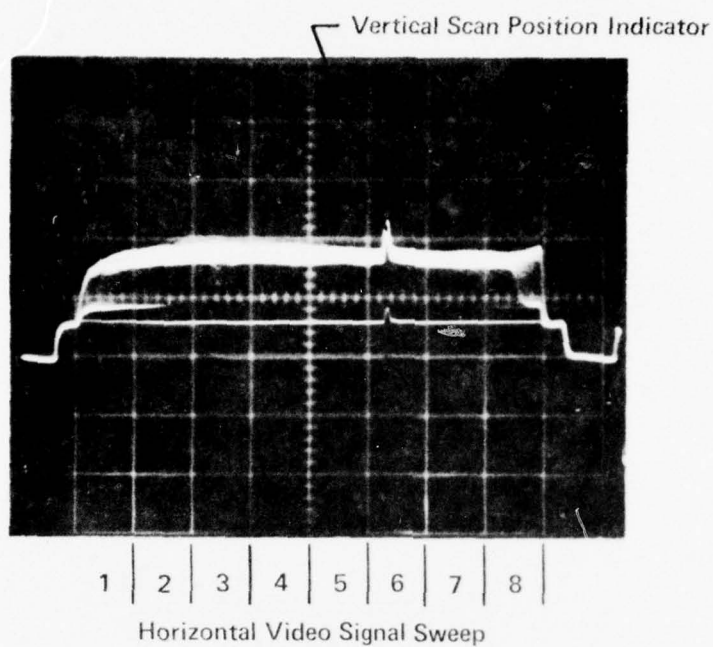


Figure 25. Vidicon grid.

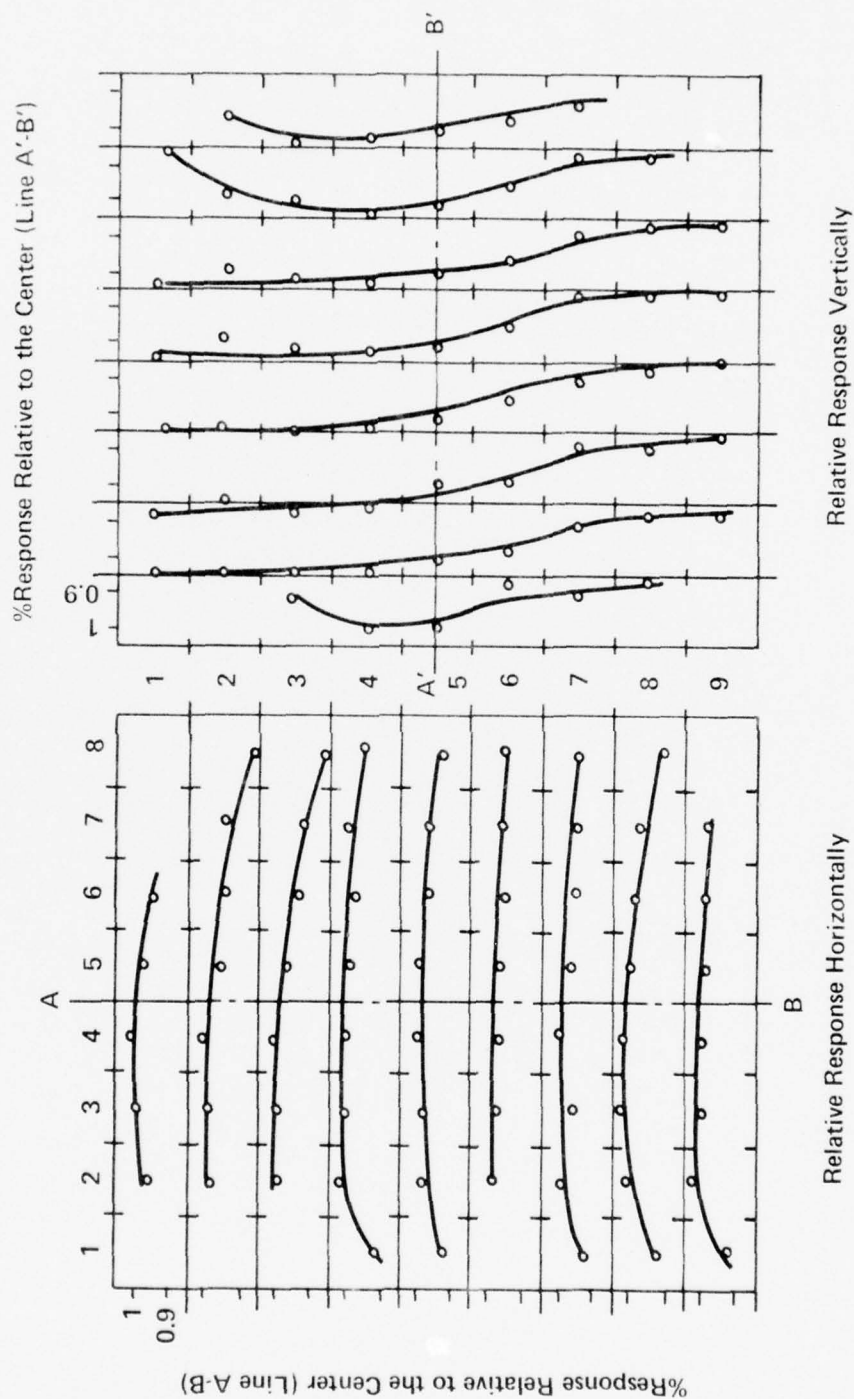


Figure 26. Vidicon response curves.

between the top and bottom portions of the picture, or Vidicon tube, a correction had to be made to the levels in the lower sectors.

Calibration Curves

The curve produced in Figure 5 is in effect the calibration curve for a Schlieren system. By increasing the transducer voltage, which is a measure of the Raman-Nath parameter, and measuring the corresponding light intensities, similar curves were obtained and are shown in Figure 27. These curves indicate the range of transducer voltages that lie in the Raman-Nath region. Therefore, using these curves, the light intensity at any point in a Schlieren image can be related to a corresponding transducer voltage.

The calibration curves were taken in the following manner: The transducer was positioned so that its output was in the center of the light beam and thus positioned in the center of the Vidicon tube. As before, the video signal was displayed on a channel of the scope. The beam image and corresponding horizontal scope display are shown in Figure 28.

The video output level displayed on the scope was continuously monitored. The camera's output level could not exceed 1.4 volts. If the transducer voltage was too high, the scene intensity was too high and the Vidicon tube was driven into saturation. In this configuration a decrease in transducer voltage did not bring about a corresponding decrease in the camera's output signal level.

In practice, the transducer voltage was increased until the camera's signal output level was just below 1.4 volts. Thus, a change

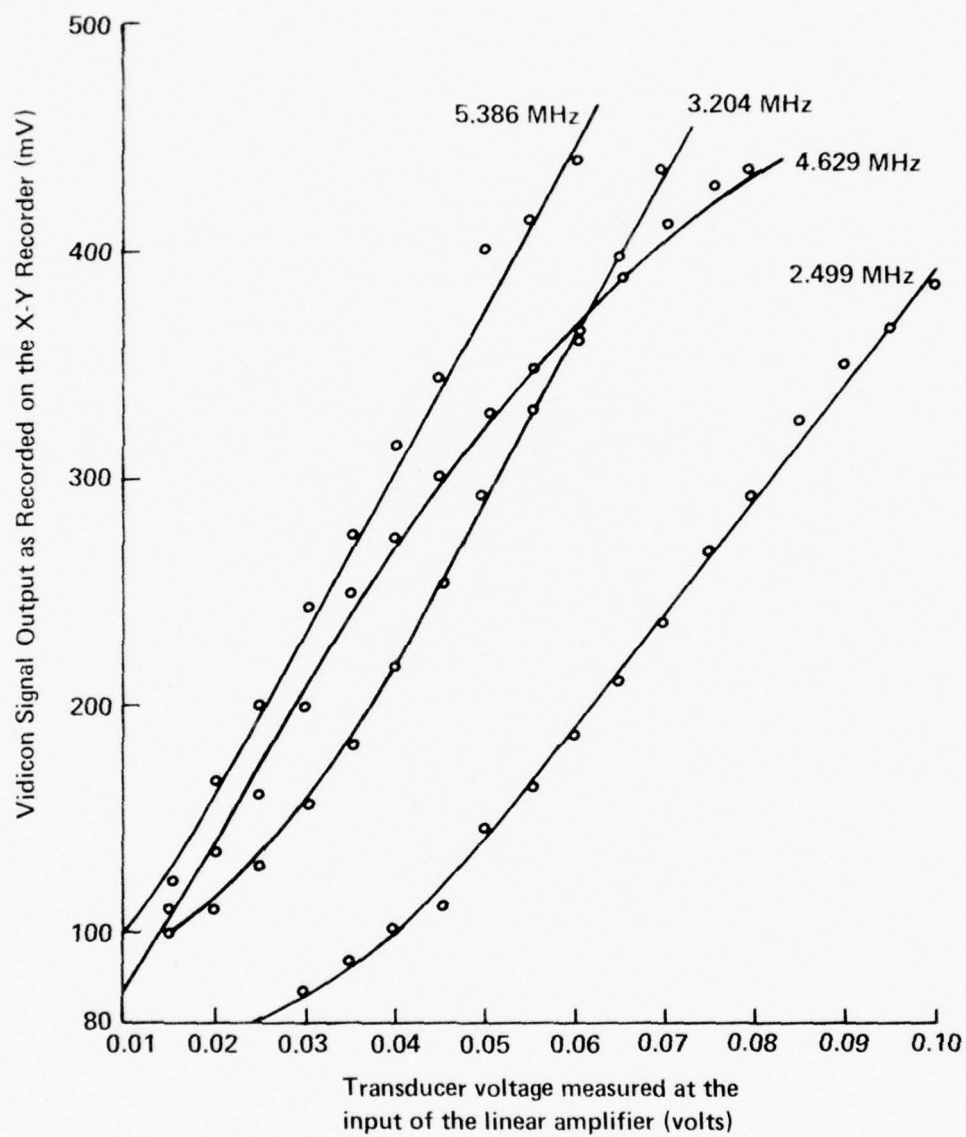
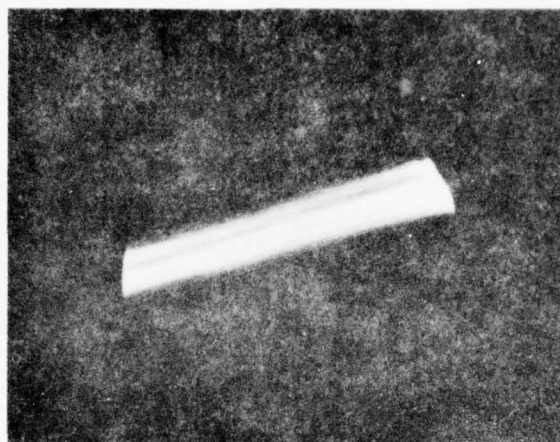
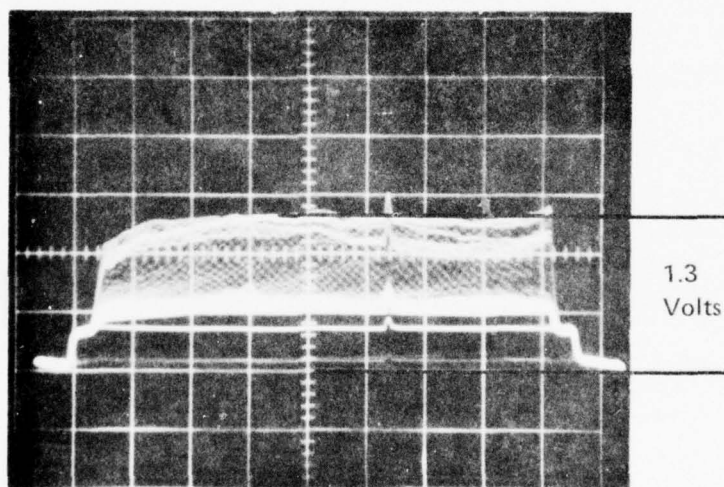


Figure 27. Calibration curves.



(a)



(b)

Figure 28. Schlieren image of a continuous 5.38 Mhz.

in transducer voltages could be detected and relative sound pressure levels determined. For Polaroid photographs and for general viewing, transducer voltages as high as the linear amplifier would deliver were used. This resulted in clear and sharp photographs and bright and uniform CCTV images.

The calibration curves (Figure 27) were taken with the highest transducer voltage that gave a composite video output of 1.3 volts. The transducer voltages were then decreased and the corresponding scene intensity recorded. The calibration curves are plots of the applied transducer voltage, measured at the input of the linear amplifier, versus the recorded intensity level taken at the center of the Vidicon tube. In a Schlieren image, intensity levels are referred to these calibration curves and voltage levels are obtained. A comparison of these voltages, which are directly proportional to the sound pressures, results in relative measurements.

The method used to drive the transducers required that a calibration curve be taken at each of the frequencies used. Also, once the opaque stop was disturbed the calibration curves had to be rechecked. This was especially true at low frequencies. Obviously it was also important that the water be kept clean.

Vidicon Tube Parameters

To obtain the Vidicon tube parameters, the Schlieren system was setup in the same way as for the calibration curves, with a single acoustic beam imaged at the center of the Vidicon tube. The transducer voltage was set to give a camera output level of 1.3 volts. Neutral

density filters were placed in the light beam and the corresponding decrease in the camera's signal output level was recorded on the X-Y recorder. The result was in the series of transfer curves produced in Figure 17.

An Example of Quantitative Schlieren Measurements

In a recent report, Hayek (1974) discusses the high-frequency backscattering and transmission from thick elastic plates. Using the Mindlin plate theory, Hayek calculates the reflection and transmission coefficients at insonifying frequencies above the coincidence frequency. These are written as

$$R = \frac{\frac{Z}{\rho c'}}{2 + \frac{Z}{\rho c'}} \quad \text{and} \quad T = \frac{2}{2 + \frac{Z}{\rho c'}}$$

with $\Omega = \frac{\omega'}{\omega_0}$

The reflection and transmission curves for various Ω 's are given in Figures 29 and 30.

These curves were used to check the accuracy of the Schlieren system and its method of obtaining quantitative measurements. A 0.004-inch thick steel plate with a coincidence frequency of 2.48 Mhz was insonified in the water tank at frequencies above the coincidence frequency. The experimental procedure was as follows: In order to have the acoustic beam image uniform across the face of the Vidicon tube, the sound beam had to be perpendicular to the light beam. This could be done visually; however, a more convenient method was possible. With the video signal output displayed on one channel of the scope (as

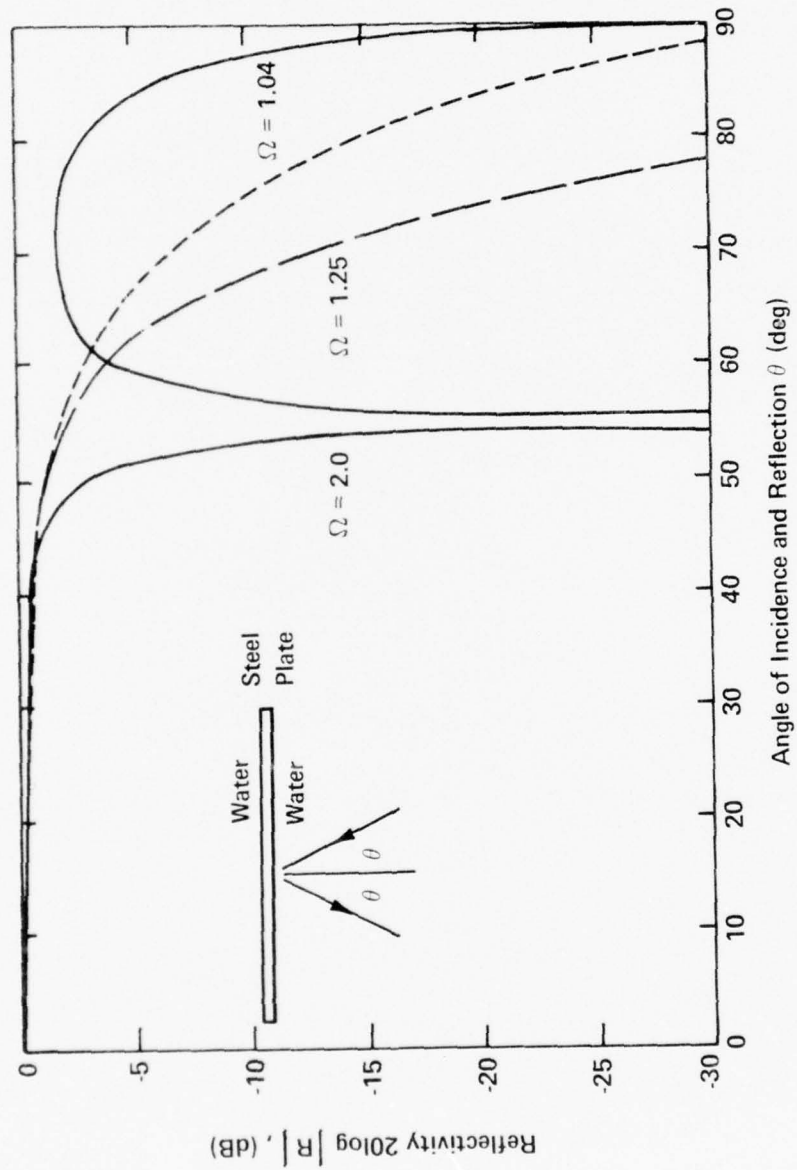


Figure 29. Reflectivity (Mindlin plate theory).

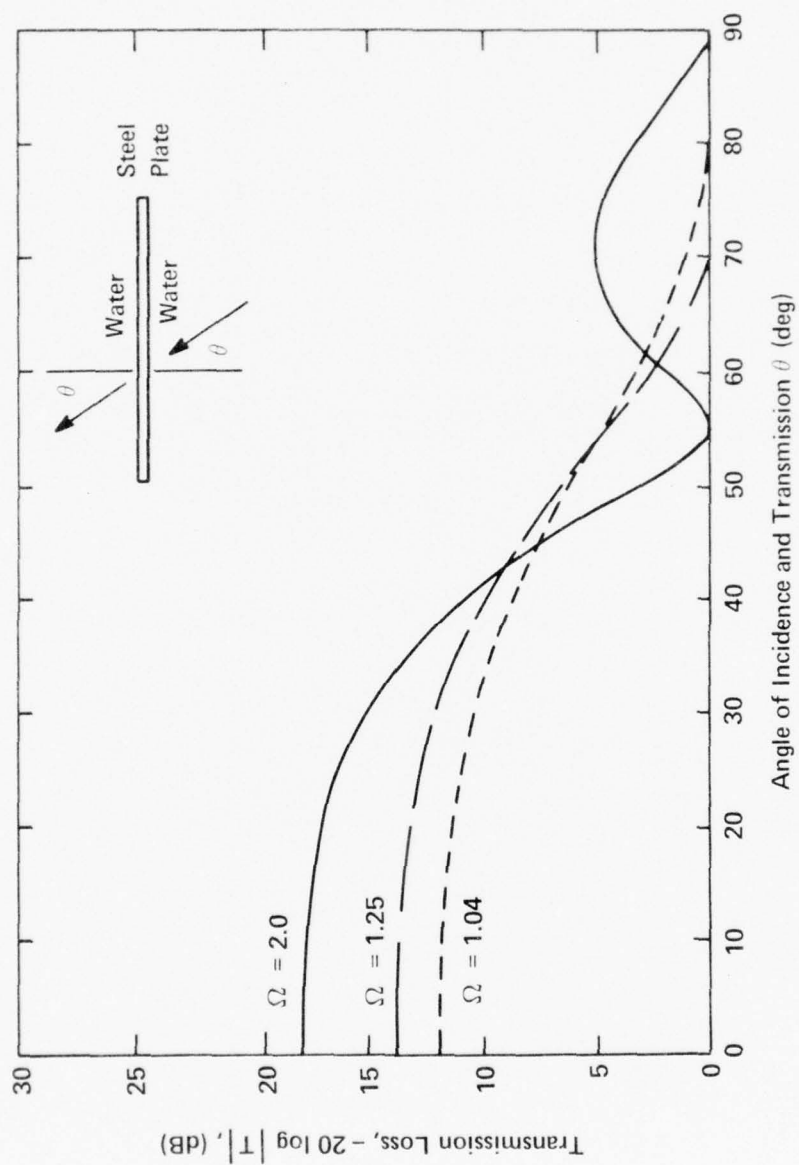
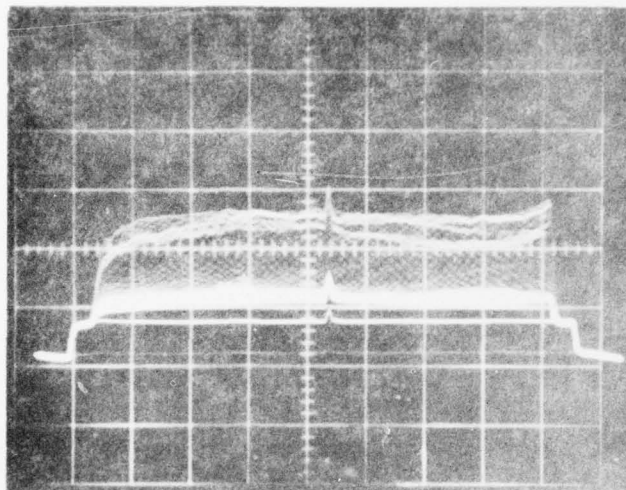


Figure 30. Transmission loss (Mindlin plate theory).

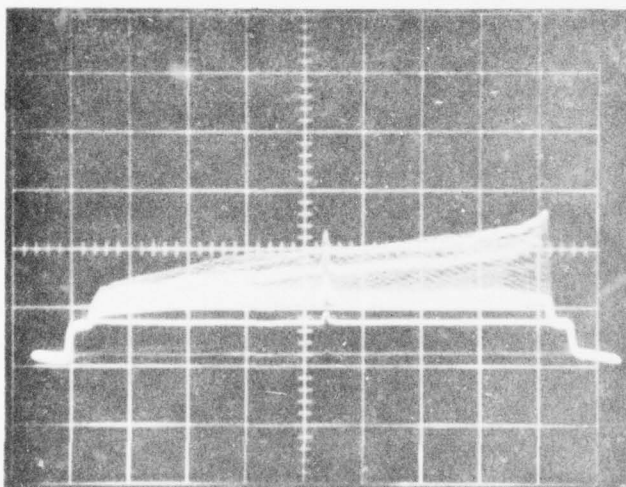
previously done), the transducer position was adjusted so that the horizontal signal sweep display appeared as in Figure 31a. This was consistent with a uniform image across the field of view and with the symmetry of the diffraction orders. Shown in Figure 31b is the horizontal sweep for the image intensity when the acoustic beam was not perpendicular to the light beam.

The insonified thin plate was adjusted so that the horizontal signal sweep appeared as in Figure 32. This insured that the incident, transmitted and reflected acoustic beam image intensities were uniform across the field of view. The steel plate insonified at various angles of incidence is shown in Figures 33 and 34. Vertical intensity scans were taken across each of the incident, reflected and transmitted beams. The horizontal and vertical positions of the intensity scans were recorded and the percent correction to the intensity level due to the varied response of the Vidicon surface was calculated. In practice, only the intensity levels which fell into grid squares having a difference in response of at least 5% were corrected. The reason being that a 3 to 4% difference from measurement to measurement was apparently due to fluctuations in the transient recorder's digital converters and the camera's video signal. In most cases corrections were only needed to the reflected intensity levels since they fell into the lower portion of the Vidicon tube's field of view. The corrections to the reflected intensity levels were on the order of 10 to 15%.

The corrected and uncorrected points were referred to the calibration curves, and the results of the intensity scans taken at different angles and different Ω 's are illustrated in Figures 35, 36, and 37.

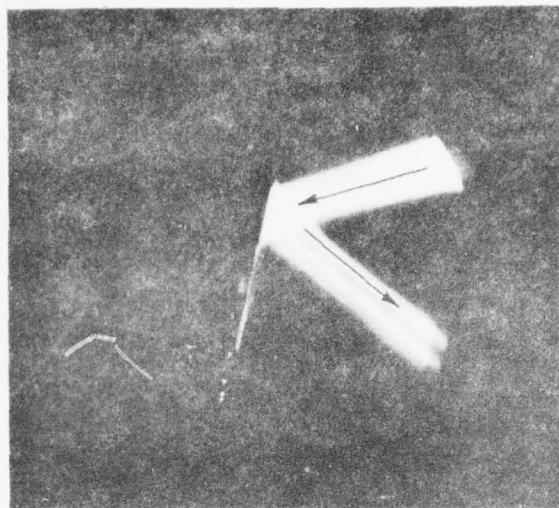


(a)

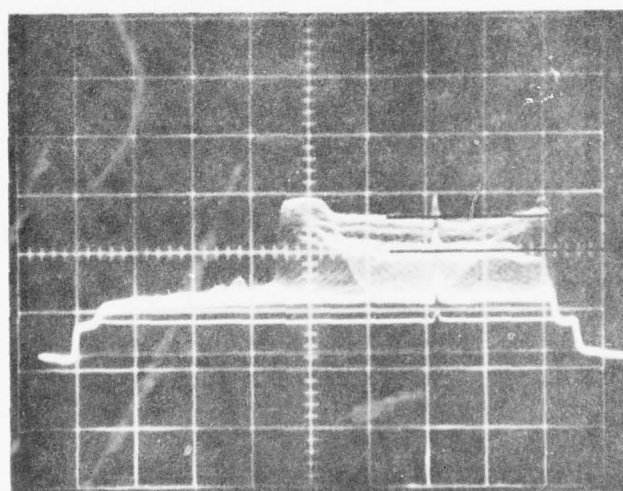


(b)

Figure 31. Horizontal video signal. (a) Acoustic beam perpendicular to the light beam. (b) Acoustic beam not perpendicular to the light beam.



(a)

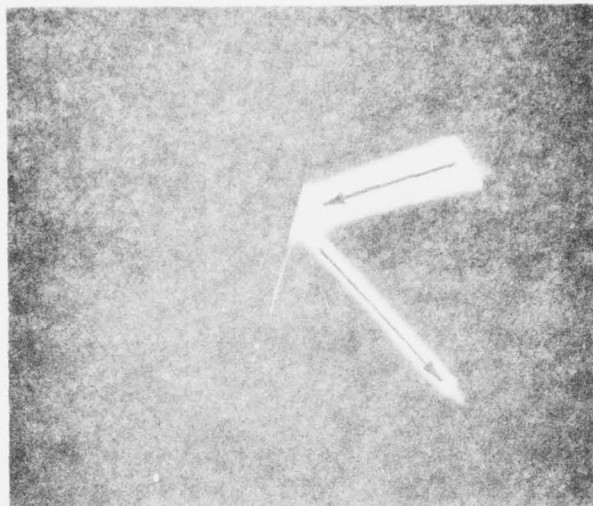


Incident
Level

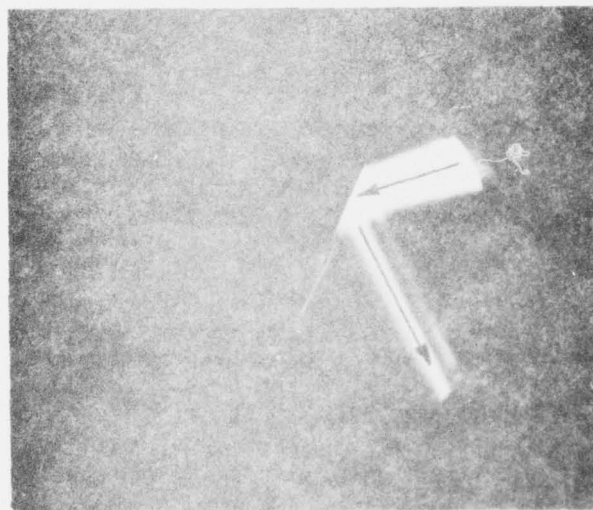
Reflected
Level

(b)

Figure 32. (a) Schlieren image of a steel plate insonified by 4.62 Mhz acoustic beam. (b) Horizontal video signal display showing uniform incident and reflected intensity levels.

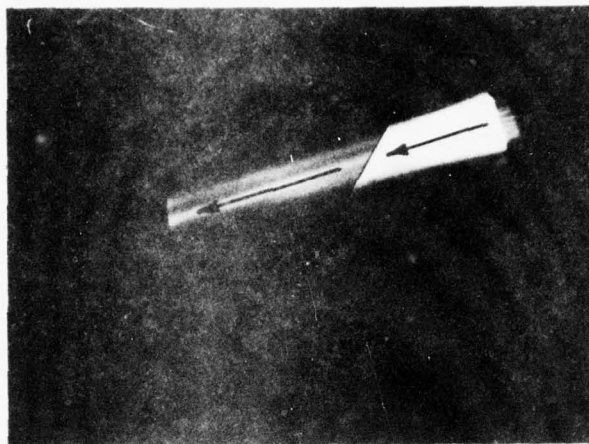


(a)

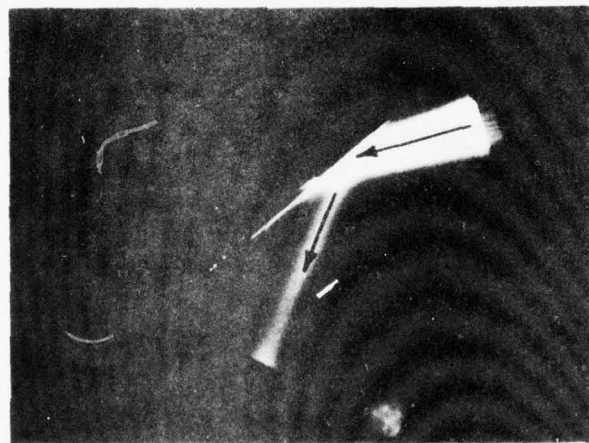


(b)

Figure 33. Schlieren images of a steel plate insonified at 5.3 Mhz and at different angles of incidence: (a) 30°; (b) 40°. Plate coincidence frequency = 2.5 Mhz.



(a)



(b)

Figure 34. Schlieren images of a steel plate insonified at 5.3 Mhz and at different angles of incidence: (a) 50°; (b) 65°. Plate coincidence frequency = 2.5 Mhz.

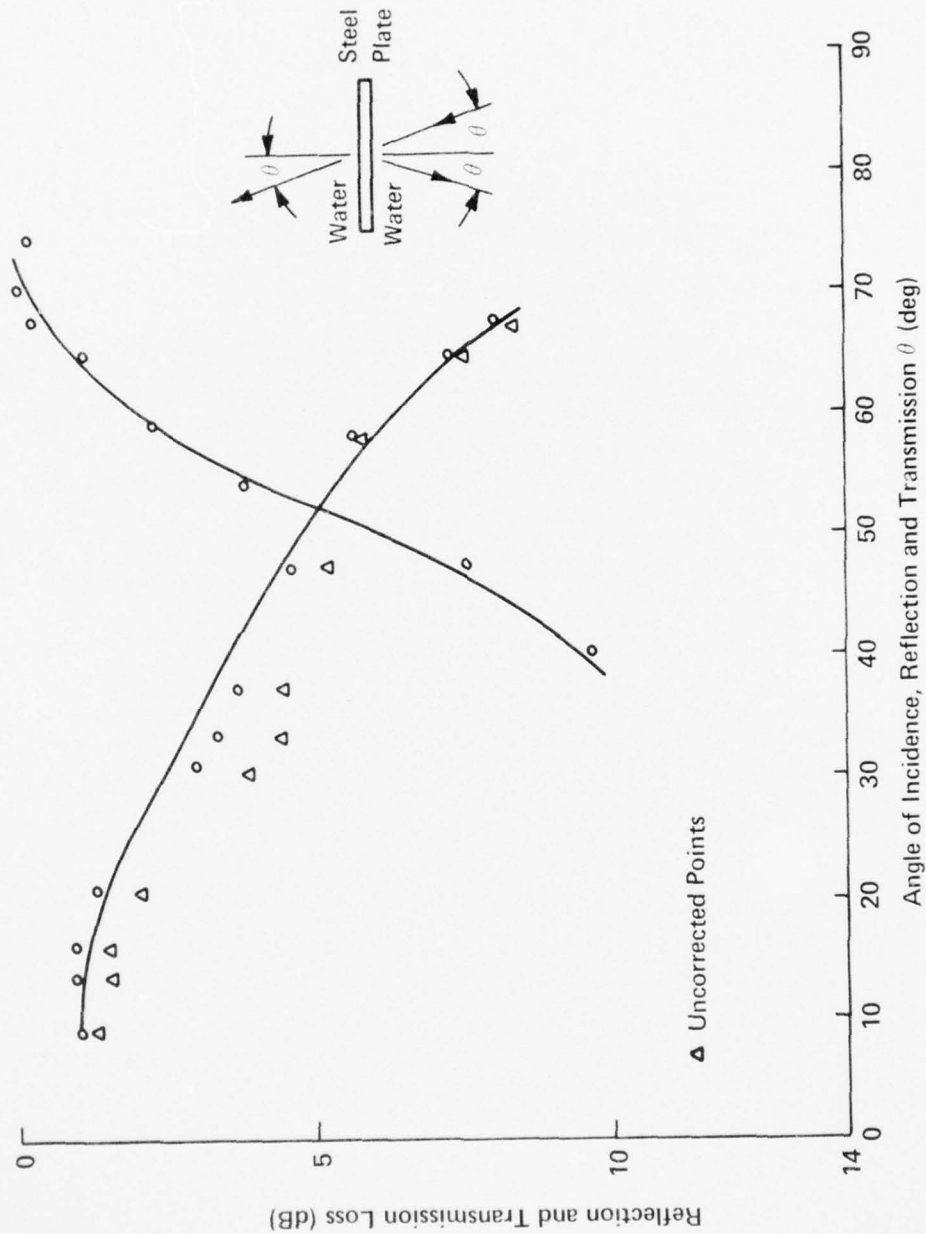


Figure 35. Reflection and transmission loss for $\Omega = 1$.

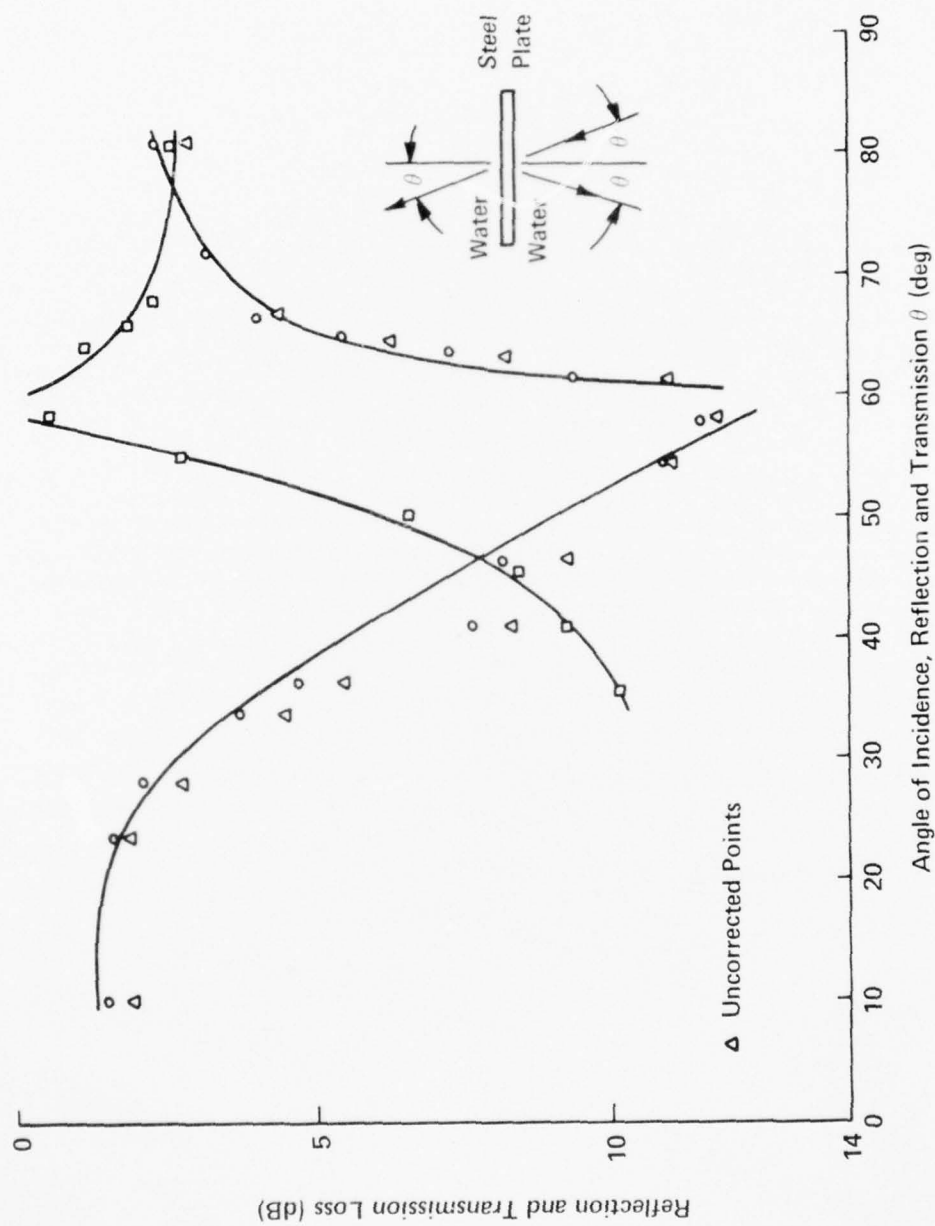


Figure 36. Reflection and transmission loss for $\Omega = 1.35$.

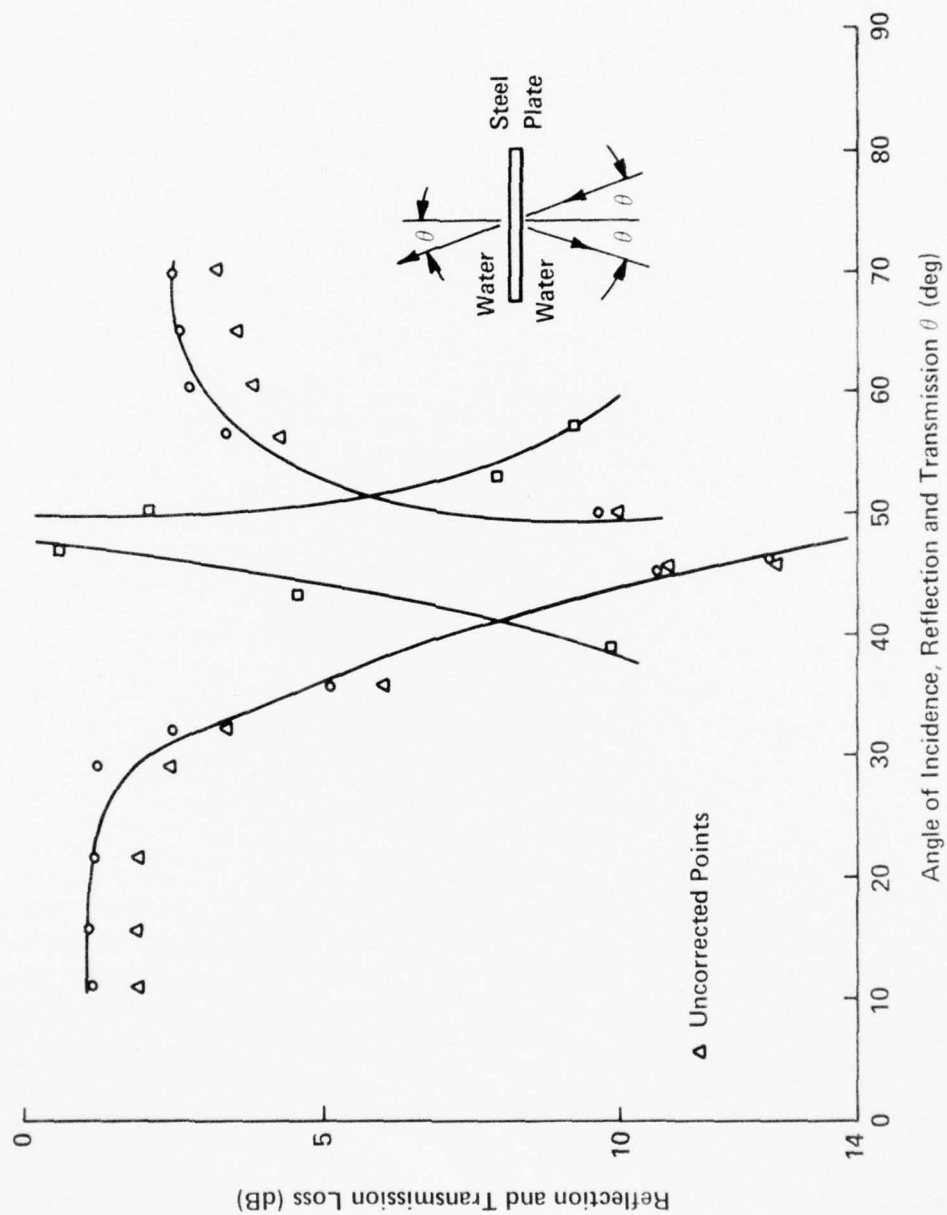


Figure 37. Reflection and transmission loss for $\Omega = 2.1$.

As can be seen, the corrected and uncorrected points differed by at most 2 dB. When these curves are compared to those in Figures 29 and 30, it is clear that this method of obtaining quantitative sound pressure information directly from a Schlieren image has met with spectacular results.

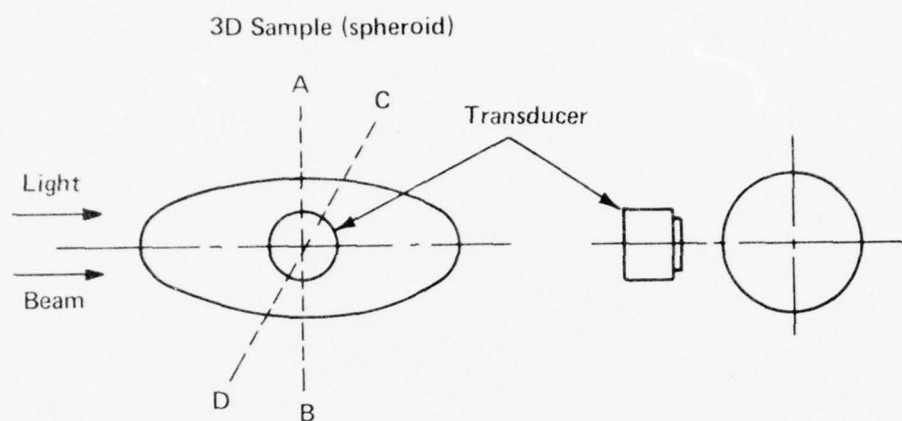
Three-Dimensional Schlieren Information

A method to obtain three-dimensional quantitative information directly from a Schlieren image was also devised. The sound field that is imaged in a Schlieren system is due to pressure disturbances in a plane perpendicular to both the sound beam and the light beam. However, when insonifying a complex structure, there is scattering and transmissions in all angular directions. Figure 38 shows a method by which the information appearing in any angular direction can be imaged and quantitatively analyzed.

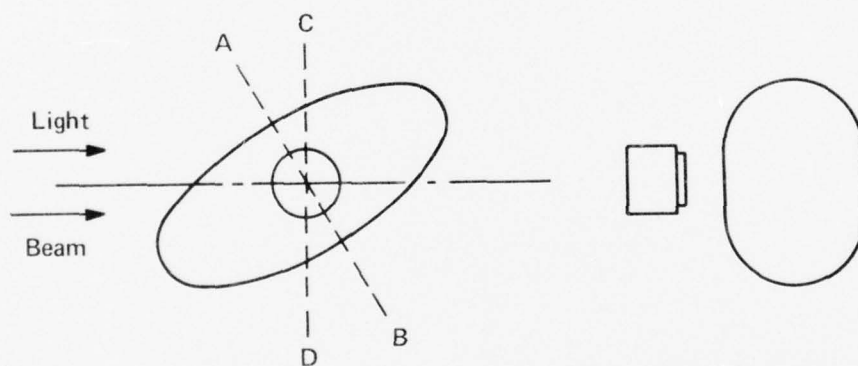
The method consists of constructing a positioner that would rigidly rotate the transducer and the sample in the light beam. Thus, acoustical scattering in other angular planes can be brought into the imaging plane that is perpendicular to the light beam and acoustic beam. No data is presented as the above discussion is intended only to demonstrate that three-dimensional problems can be visualized in a Schlieren system.

Diffraction and Transmission for an Aluminum Wedge

Schlieren images of a 60° aluminum wedge insonified by a 4.62 Mhz acoustical beam are shown in Figures 39 and 40. The sound beam and the wedge were positioned as in the previous examples, of the insonified



Scattering in plane A-B which is perpendicular to the light beam is the only plane imaged in a Schlieren system. However, there is scattering also in plane C-D which is not imaged.



Sample and transducer rotated to bring scattering in plane C-D into view.

Figure 38. Three-dimensional Schlieren system.

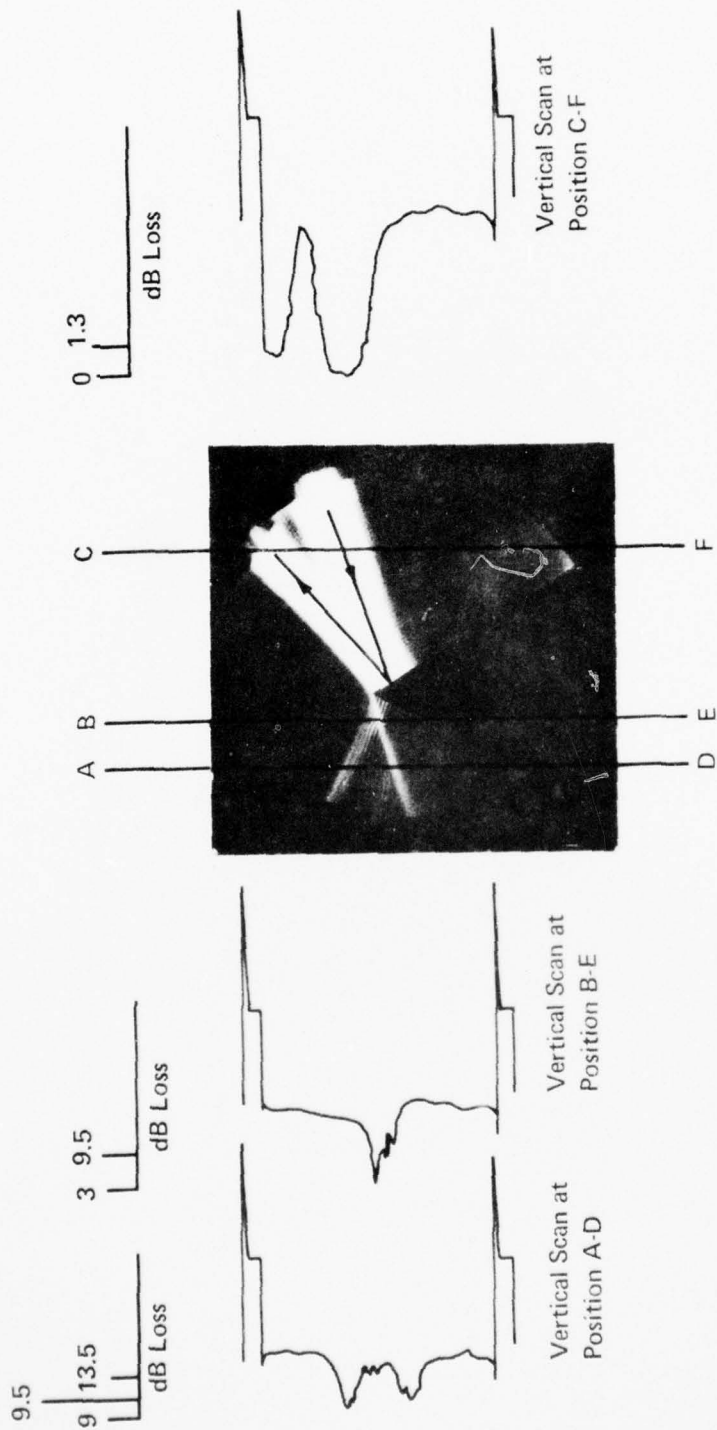


Figure 39. Reflection, transmission and diffraction for a 60° aluminum wedge insonified at 4.62 Mhz with the angle of incidence = 10°.

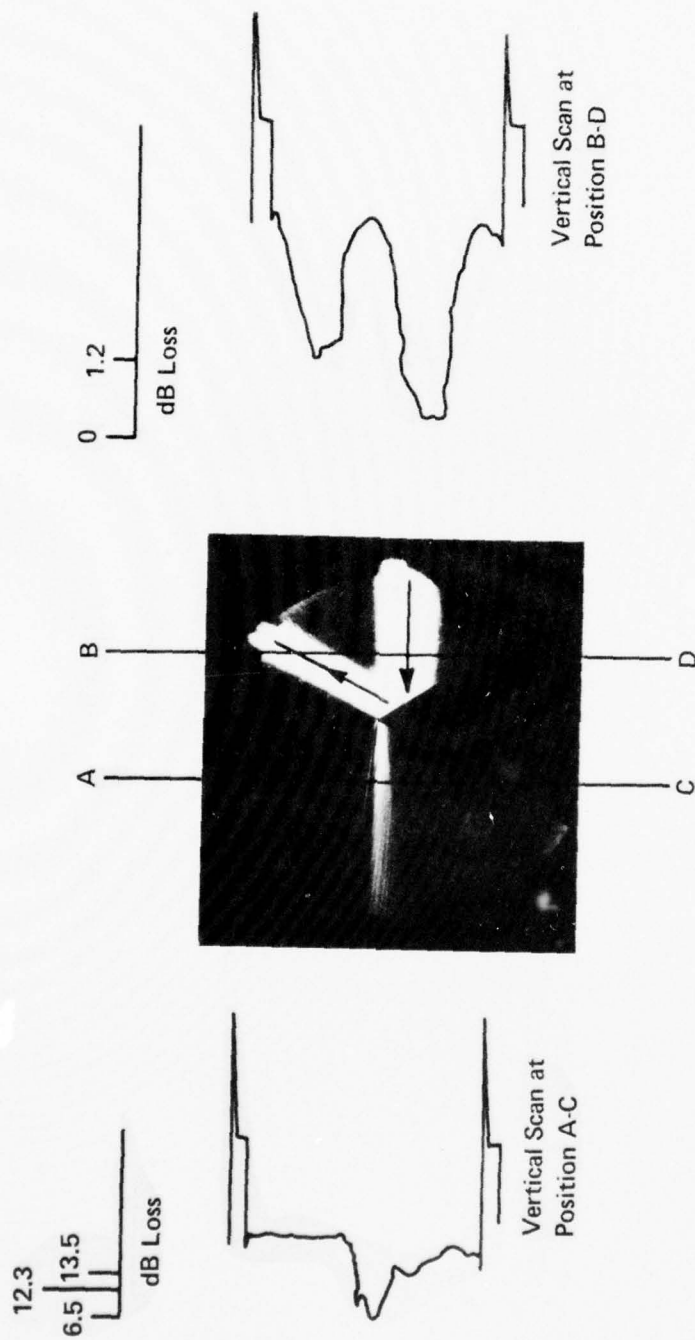


Figure 40. Reflection and transmission for a 60° aluminum wedge insonified at 4.62 Mhz with the angle of incidence = 30°.

plate, for the most uniform image intensity across the field of view. However, this did not appear possible for the transmitted beam, since only a small portion next to the wedge appeared with uniform image intensity. At this point no reason can be given for this phenomenon other than it appears that the ray size in the transmitted beam is at the size resolution limit of the CCTV camera.

The spectral reflections, transmission, and diffraction of the incident acoustic beam were clearly visible. Vertical intensity scans were taken at the positions indicated and the values referred to the appropriate calibration curve. The results are shown next to the Schlieren images.

Acoustic Transmission and Reflection from Concentric Cylinders

Figure 41 shows two concentric cylinders insonified by a 4.62 Mhz acoustic beam. Vertical intensity scans were taken at the positions shown and the results are plotted beside the Schlieren image.

Spectral Reflection from a Prolate Spheroid

A 4.62 Mhz acoustical beam insonifying an aluminum prolate spheroid is shown in Figure 42. There is very directional spectral reflection at about 20° and for several degrees on either side of this angle of incidence. Vertical image intensity scans were taken at the positions shown and the results indicated that this spectral reflection decreased by about 12 dB. This decrease appears to be consistent with the low level of acoustic spectral reflections previously observed from a spheroid. However, the strong directional reflection at a specific range of incidence was unexpected.

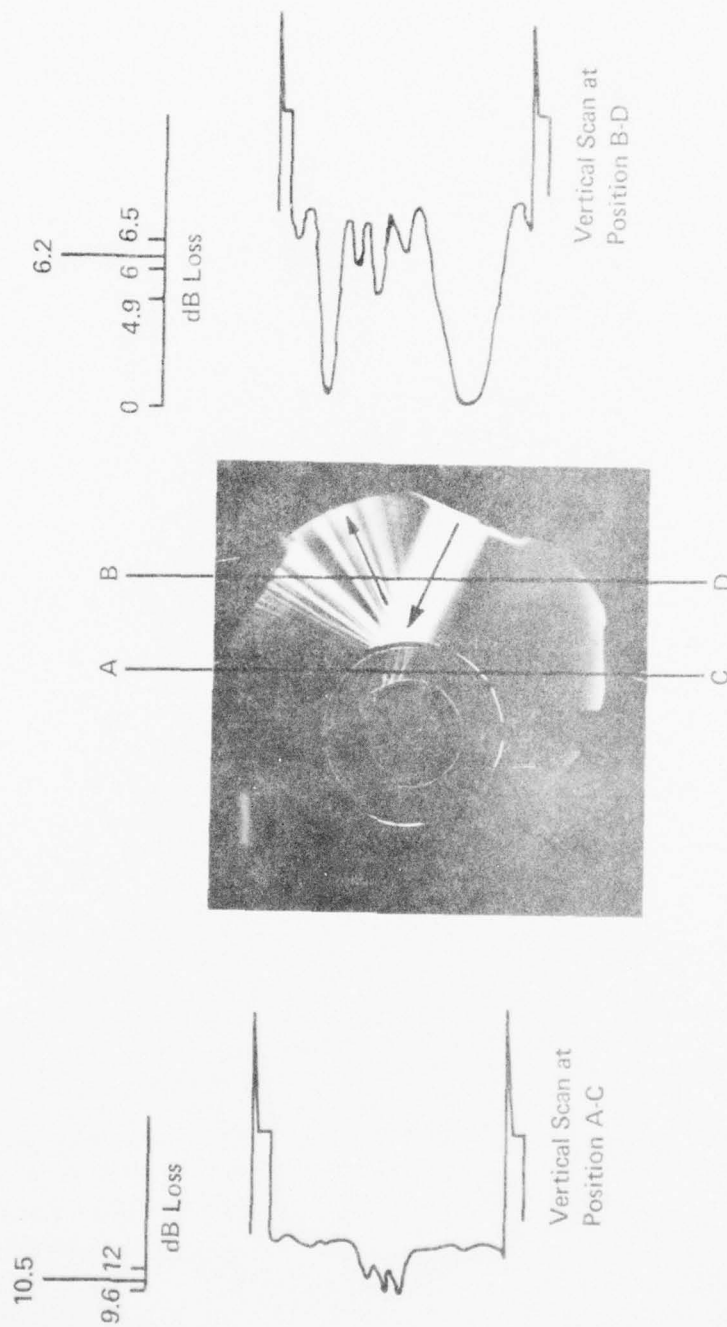


Figure 41. Reflection and transmission for concentric aluminum cylinders insonified at 4.62 Mhz with the angle of incidence = 35° .

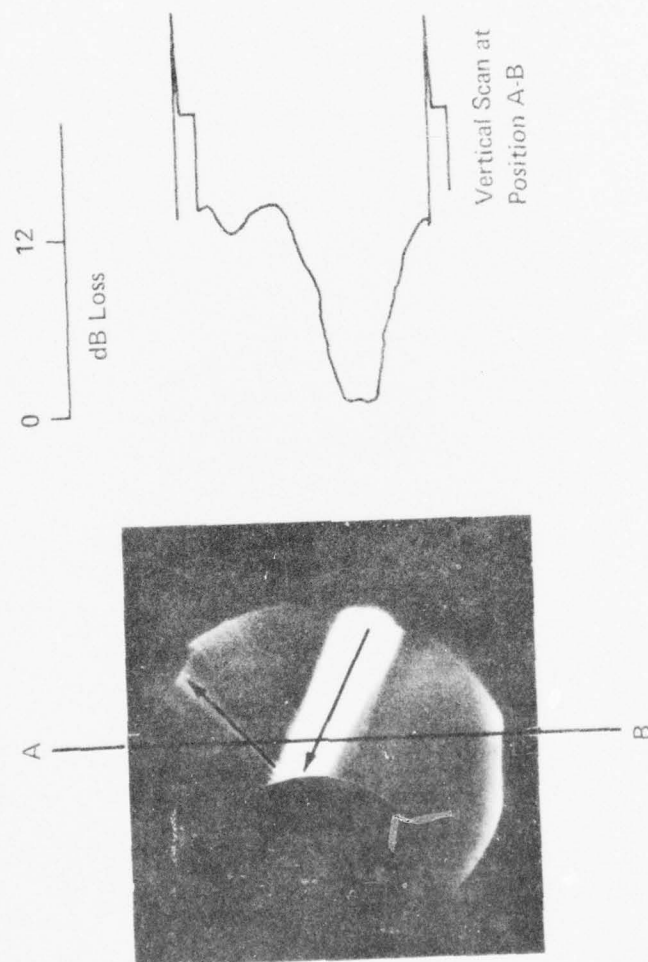


Figure 42. Spectral reflection from an aluminum prolate spheroid insonified at 4.62 Mhz with the angle of incidence = 20° .

Transmission and Reflection from a Welded Steel Plate

Two steel plates were welded together and insonified by a 4.62 Mhz acoustic beam. The result shown in Figure 43 indicates an abnormally large amount of transmission through the welded joint. This was the first time that this type of acoustic transmission had been observed and at present it is not completely understood.

A Ribbed Steel Plate Insonified by a Short Acoustic Pulse

Because of the lower flash synchronization rate and the correspondingly higher light output of the xenon tube, it was necessary to take a new calibration curve for each of the acoustic frequencies used. After the pulse image had been aligned in the same manner as the continuous sound beam, vertical intensity scans were taken at the brightest and most uniform part of the pulse image, and for various transducer voltages. The resulting calibration curve for a 4.62 Mhz, 30- μ sec long acoustic pulse is shown in Figure 44.

Figures 45 through 50 show a ribbed steel plate insonified by a 4.62 Mhz, 30 μ sec long acoustic pulse. Note the strong spectral reflection back in the direction of the incident pulse. The results of the vertical image intensity scans are shown beside each Schlieren image. Each of the images were taken 10 μ sec later in time.

AD-A034 451

PENNSYLVANIA STATE UNIV UNIVERSITY PARK APPLIED RESE--ETC F/G 20/1
QUANTITATIVE SCHLIEREN VISUALIZATION.(U)

UNCLASSIFIED

OCT 76 S STANIC
TM-76-279

N00017-73-C-1418
NL

2 OF 2
ADAO34451



END

DATE
FILMED
2 - 77

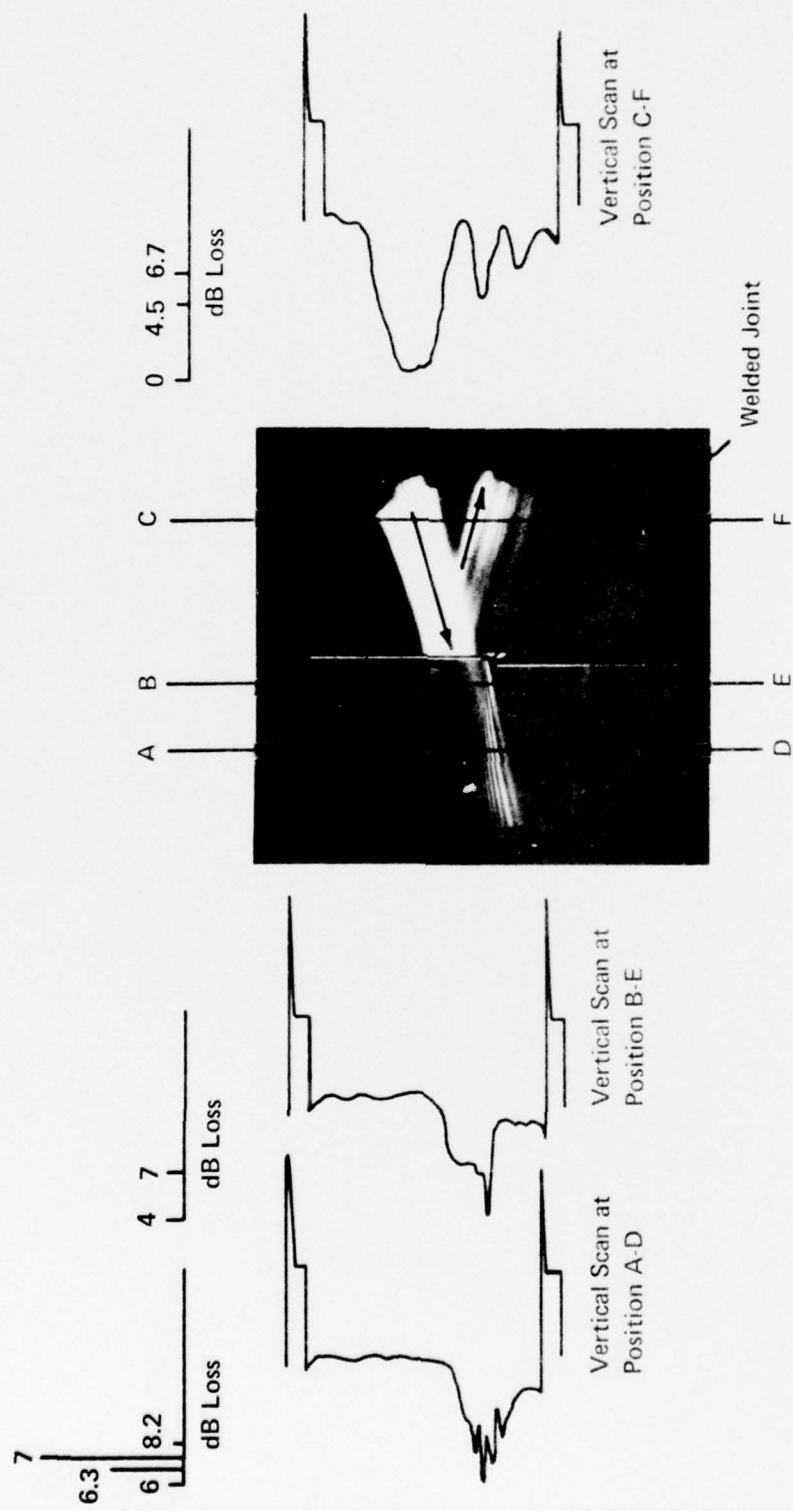


Figure 43. Reflection and transmission for two steel plates welded together and insonified at 4.62 Mhz with the angle of incidence = 15°.

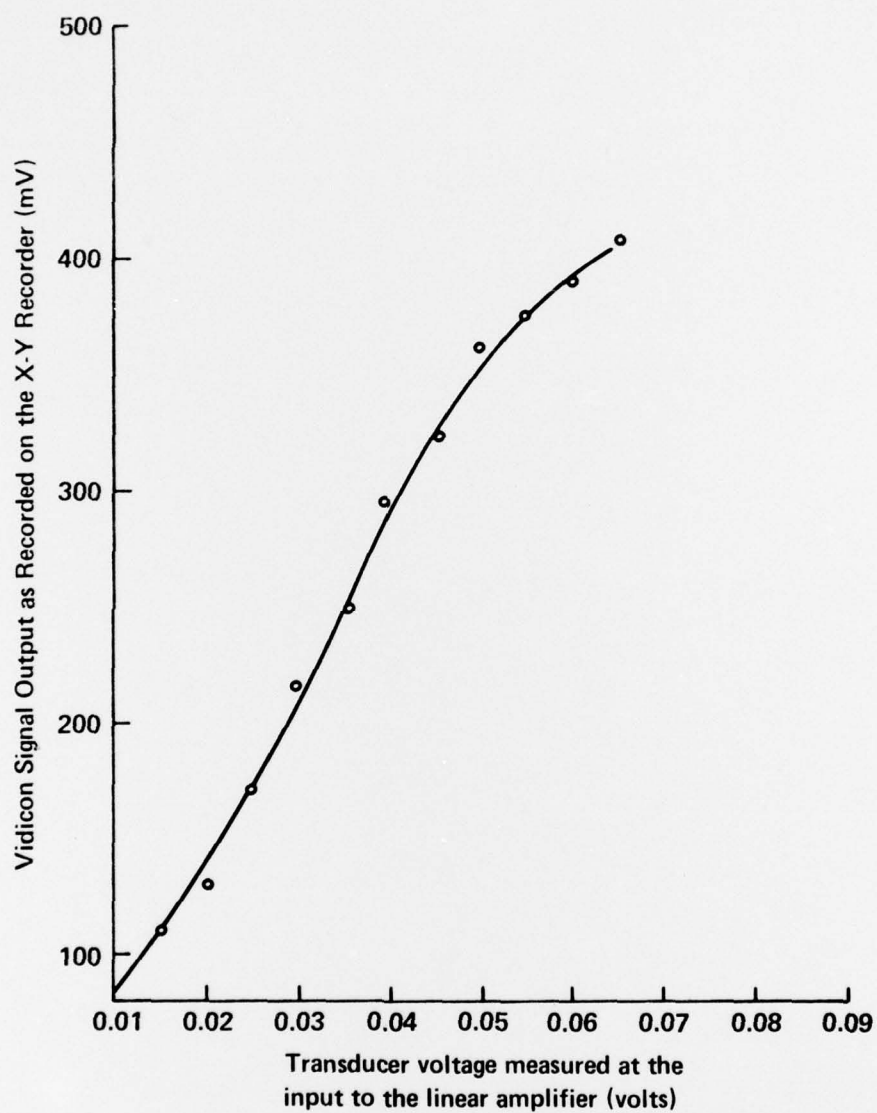


Figure 44. Calibration curve for a 30- μ sec long 4.62 Mhz pulse

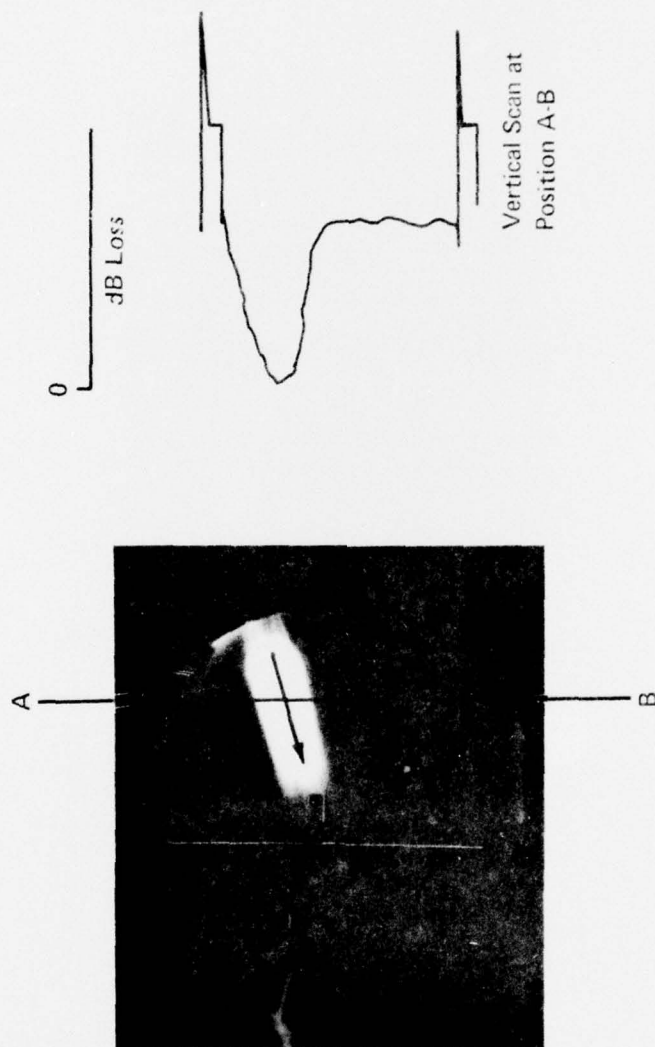


Figure 45. A thin steel plate with a steel rib welded on one side insonified by a 30- μ sec long, 4.62 Mhz acoustic pulse with the angle of incidence = 15° . Time = T_1 .

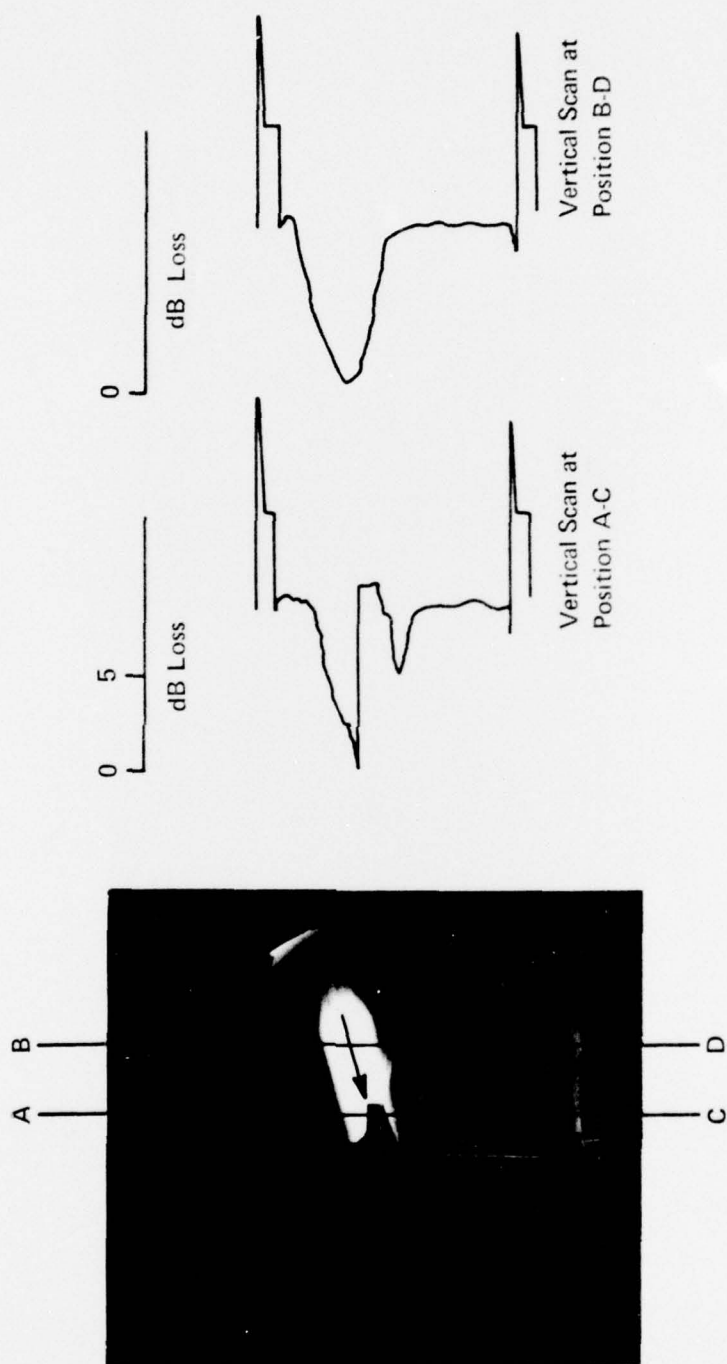


Figure 46. A thin steel plate with a steel rib welded on one side insonified by a 30- μ sec long, 4.62 Mhz acoustic pulse with the angle of incidence = 15° . Time = $T_1 + 10 \mu\text{sec}$.

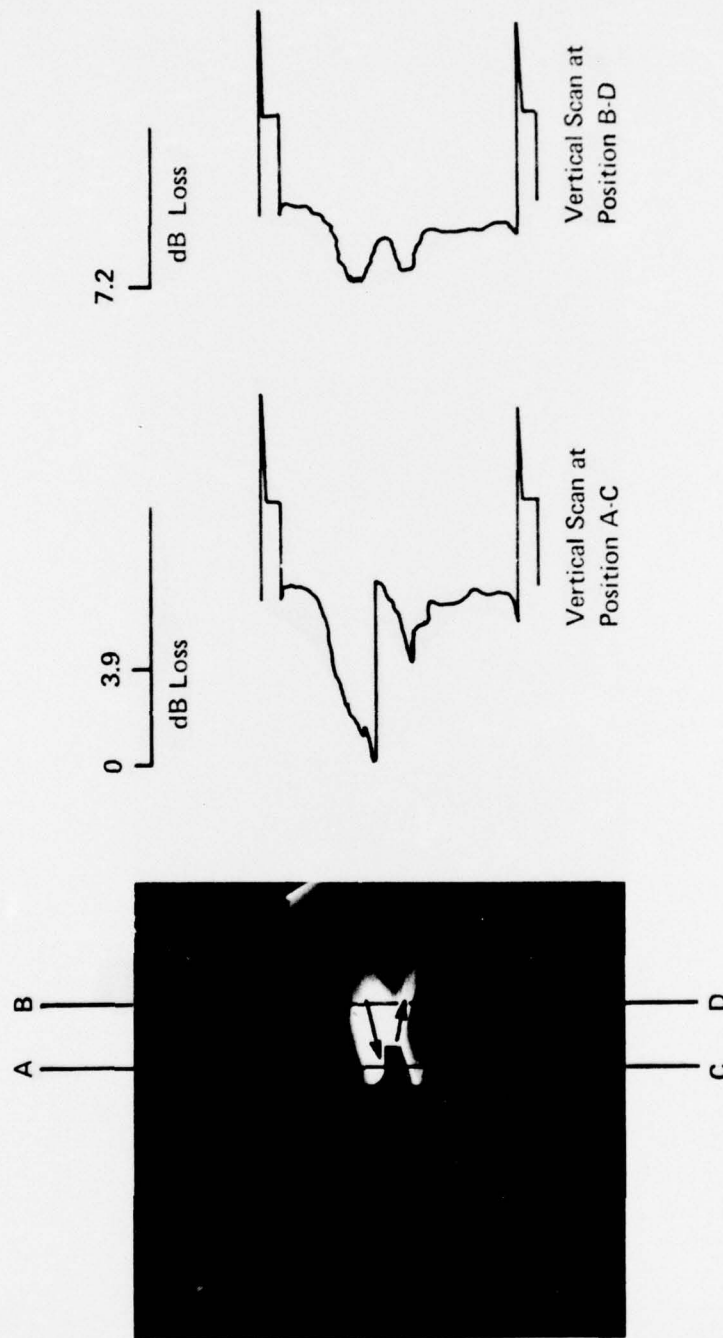


Figure 47. A thin steel plate with a steel rib welded on one side insonified by a 30- μ sec long, 4.62 Mhz acoustic pulse with the angle of incidence = 15° . Time = $T_1 + 20 \mu$ sec.

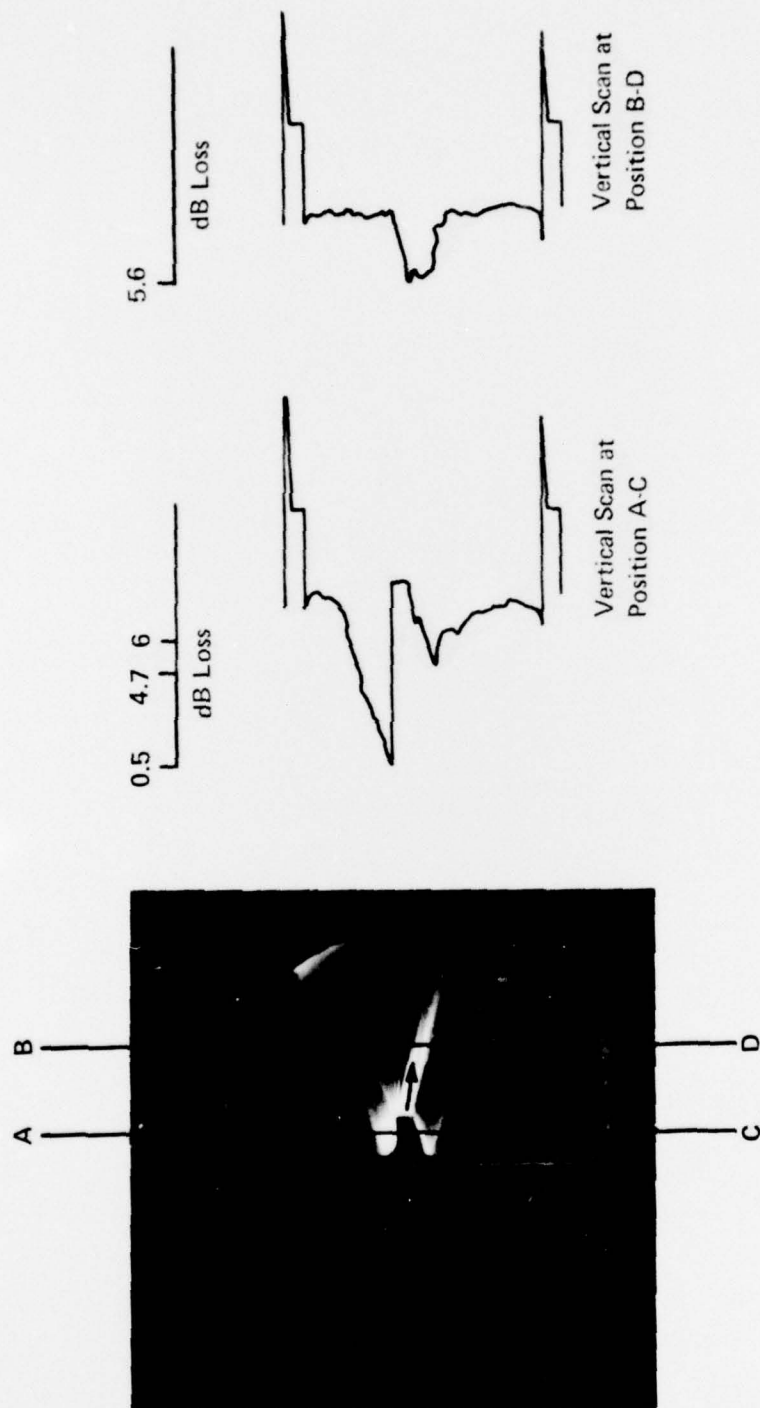


Figure 48. A thin steel plate with a steel rib welded on one side insonified by a 30- μ sec long, 4.62 Mhz acoustic pulse with the angle of incidence = 15° . Time = $T_1 + 30 \mu$ sec.

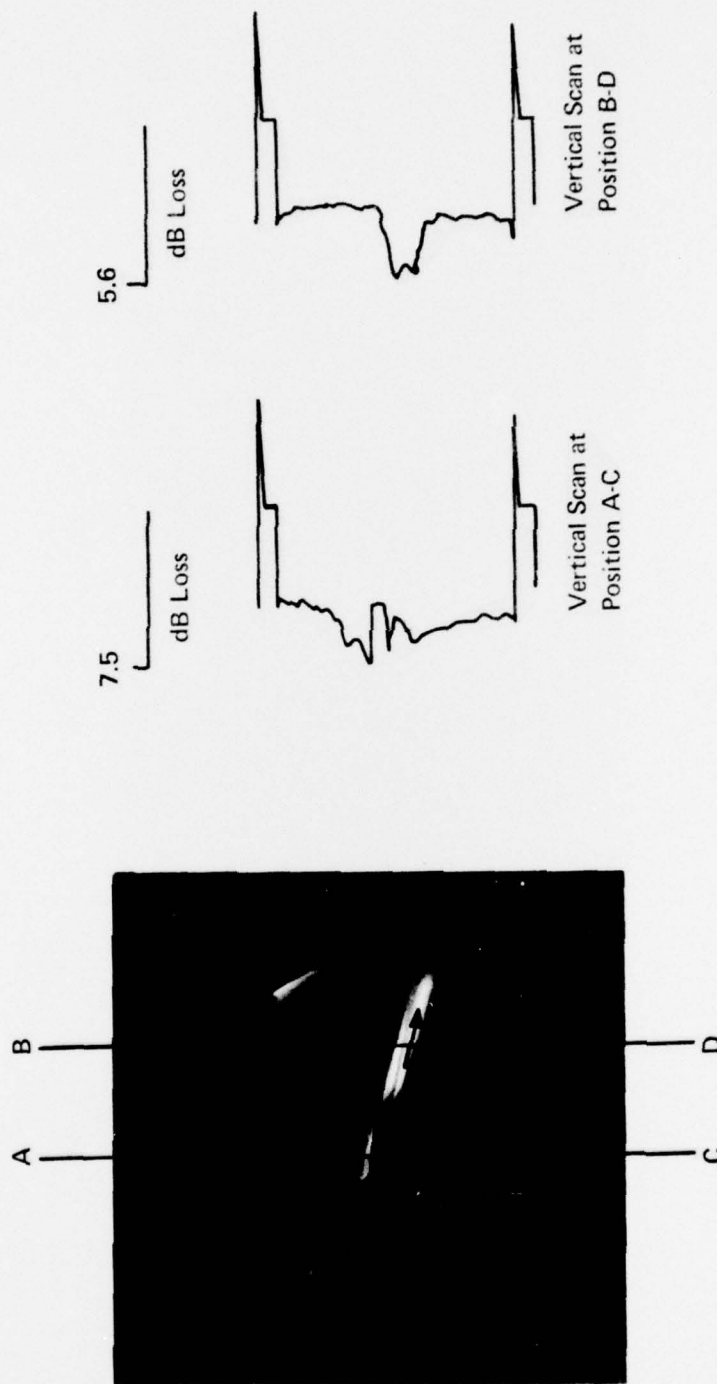


Figure 49. A thin steel plate with a steel rib welded on one side insonified by a 30- μ sec long, 4.62 Mhz acoustic pulse with the angle of incidence = 15° . Time = $T_1 + 40 \mu$ sec.

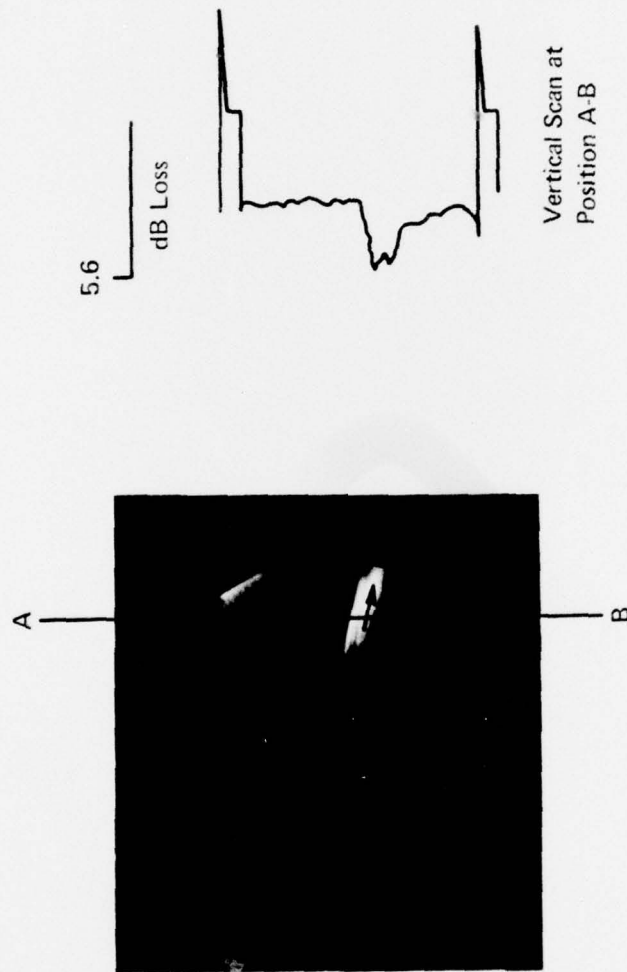


Figure 50. A thin steel plate with a steel rib on one side insonified by a 30- μ sec long, 4.62 Mhz acoustic pulse with the angle of incidence = 15° . Time = $T_1 + 50 \mu$ sec.

VI. SUMMARY AND CONCLUSIONS

Using a closed circuit television camera (CCTV), a method was developed to directly obtain quantitative sound pressure measurements from the sound fields imaged in a Schlieren system.

By using the exact timed format of the composite video signal and a series of time delay circuits, it was possible to take vertical intensity scans of a Schlieren image at any position on the television raster. The method used the camera's horizontal blanking pulse to trigger a broadband, high-speed sample-and-hold amplifier. This amplifier was triggered to sample each of the horizontal scan lines at a selected time in the horizontal scan sweep and to feed this value into a transient recorder. The signal was digitized and a continuous analog voltage signal corresponding to the black-white information from a Schlieren image was displayed on a scope. The same analog signal was also plotted on an X-Y recorder.

The ease with which the Schlieren system can be operated is evident from the fact that only a single calibration curve at each frequency was needed. The curves plotted applied transducer voltage against the video output level. Thus, by comparing the video output levels for several vertical image intensity scans on a Schlieren image, relative sound pressure measurements were routinely obtained.

This investigation also demonstrated that in a high-quality Schlieren system, lenses of the best quality must be used. The higher the quality of the lens, the sharper the image of the light source and the better the resolution between the zeroth and the first diffraction orders.

In practice, a Schlieren system must also have a long focal length lens to resolve the zeroth and the first diffraction orders. But this results in a large and slightly dim Schlieren image. A considerable improvement was obtained by using several short focal length lenses right behind the opaque stop to allow the Schlieren image to be focused directly on the small face of the Vidicon tube's photosensitive surface. This results in an extremely bright and high-quality Schlieren image. In all cases where quantitative data was taken, the transducer was operated at a low driving voltage so as not to saturate the Vidicon tube.

The difference between using a slit and a pinhole as the source was also investigated. Although the slit resulted in a brighter Schlieren image, its use was limited to certain configurations. The pinhole was found to be the best source shape. It could be used at all acoustic angles of incidence and thus was chosen for the imaging in this study.

Future Work

It is believed that the Schlieren system can be improved in several ways. A new transducer arrangement should be devised that would have a beam with a more uniform cross-sectional intensity. A more precise transducer positioning apparatus should also be constructed. These would ensure a uniform acoustic beam at all angles of incidence.

The output of the transient recorder could be connected to a small computer and the calibration curves and Vidicon characteristics could

be stored in its memory. In this way, vertical intensity scans of a Schlieren image could be compared and the results pictured on a video display.

An additional improvement would be to change the television imaging tube to one which is linear and would accept a higher range of image intensity levels than the present 17 dB. The Plumbicon and the Tivicon are such tube types. An interesting change would be the use of a thousand-line television system which would give superb picture detail and could be used with the present system of analysis.

Greater care must be taken in constructing the Schlieren samples. Surfaces have to be kept smooth and all angles kept close to 90° . These inconsistencies were believed to have been responsible in some cases for the difficulty in positioning samples so that the transmitted and reflected beams had a uniform intensity across the field of view.

BIBLIOGRAPHY

- Bär, R., *Helv. Phys. Acta* Bd. 9, 617 (1936).
- Barnes, R. B. and Burton, Ch. J., *J. Appl. Phys.* 20, 286 (1949).
- Barone, A., *Nuovo Cim.* 7, Suppl. 2, 135 (1950).
- Bazhulin, P. A., *Trudy FIAN SSSR*, No. 5 (1948).
- Bergmann, L., *Der Ultraschall*, Chapter IV, S. Hirzel Verlag, Stuttgart (1954).
- Berry, M. V., *The Diffraction of Light by Ultrasound*, Academic Press, New York (1966).
- Bhatia, A. B. and Noble, W. J., *Proc. Roy. Soc.* 226, 356 (1953).
- Born, M. and Wolf, E., *Principles of Optics*, Chapter XII, Pergamon Press, New York (1965).
- Breazeale, M. A. and Adler, L., *J. Acoust. Soc. Amer.* 56, No. 3, 866 (1974).
- Bucaro, J. A., Flax, L., and Dardy, H. D., *J. Acoust. Soc. Amer.* 59, Suppl. 1, S8 (1976).
- Debye, P. and Sears, F. W., *Proc. Nat. Acad. Sci.* 18, 409 (1932).
- Dragonette, L. R., *J. Acoust. Soc. Amer.* 51, No. 3, 920 (1972).
- Giacomini, A., *Alta Frequenza* 7, 660 (1938).
- Hayek, S. I., Internal Memorandum, File No. 74-308, Applied Research Laboratory, The Pennsylvania State University (1974).
- Hiedemann, E. and Hoesch, K. H., *Z. Phys.* 104, 197 (1937).
- Hiedemann, E. and Osterhammel, K., *Z. Phys.* 107, 273 (1937).
- Hiedemann, E. and Zankel, K. L., *Acustica* 11, 213 (1961).
- Kang, P. and Young, F. C., *Amer. J. Phys.* 40, 697 (1972).
- Klein, W. R. and Cook, B. D., *IEEE Trans. Sonics Ultrason.* 14, No. 3, 123 (1967).
- Klein, W. R., Cook, B. D., and Mayer, W. G., *Acustica* 15, No. 2, 67 (1965).
- Klein, W. R., Tipnis, C. B., and Hiedemann, E. A., *J. Acoust. Soc. Amer.* 41, No. 1, 229 (1965).

- Korolev, F. A., Dokl. Akad. Nauk. SSSR 15, 35 (1937).
- Neeson, J. F. and Austin, S., Amer. J. Phys. 43, 984 (1975).
- Neubauer, W. G. and Dragonette, L. R., J. Acoust. Soc. Amer. 48, 1135 (1970).
- Neubauer, W. G. and Dragonette, L. R., J. Appl. Phys. 45, No. 2, 618 (1973).
- Nomoto, O., Bulletin of Kobayasi Inst. 1, No. 1, 42 (1951).
- Nomoto, O. and Negishi, K., Acustica 15, 223 (1965).
- Parthasarthy, S., Proc. Indian Acad. Sci. 3, 442 (1936a).
- Parthasarthy, S., Proc. Indian Acad. Sci. 3, 594 (1936b).
- Pierce, D. T. and Byer, R. L., Amer. J. Phys. 41, 314 (1973).
- Quate, C. F., Wilkinson, C. D. W., and Winslow, D. K., Proc. IEEE 53, No. 10, 1604 (1965).
- Raman, C. V. and Nath, N. S., Proc. Indian Acad. Sci. 2, 406 (1935a).
- Raman, C. V. and Nath, N. S., Proc. Indian Acad. Sci. 2, 413 (1935b).
- Raman, C. V. and Nath, N. S., Proc. Indian Acad. Sci. 3, 75 (1936a).
- Raman, C. V. and Nath, N. S., Proc. Indian Acad. Sci. 3, 119 (1936b).
- Seidl, F., Acta Phys. Austria 1, 155 (1948).
- Skudrzyk, E., The Foundations of Acoustics, Chapter XIII, Springer-Verlag, New York (1971).
- Smirnov, E. P., Kheifets, E. I., and Shenderov, E. L., Sov. Phys. Acoust. 19, No. 2, 159 (1973).
- Straub, H., Deutsch. med. Wochenschrift 73, 382 (1947).
- Toppler, A., Ann. Phys. 127, 566 (1867).
- Willard, G. W., J. Acoust. Soc. Amer. 21, No. 2, 101 (1949).

VITA

Steve Stanic was born on August 2, 1944 in Montreal, Canada. He graduated from Rosemount High School, Montreal, Canada in June 1962. He received the B.S. degree in Physics and Math in May 1967 from Sir George Williams University, Montreal, Canada. In September 1970 he received the M.S. degree in Aerospace Engineering from The Pennsylvania State University, University Park, Pennsylvania. In 1970 he participated in the oceanographic program at McGill University, Montreal, Canada. He is a member of the Acoustical Society of America.

DISTRIBUTION

Commander (NSEA 09G32)
Naval Sea Systems Command
Department of the Navy
Washington, D. C. 20362

Copies 1 and 2

Commander (NSEA 0342)
Naval Sea Systems Command
Department of the Navy
Washington, D. C. 20362

Copies 3 and 4

Defense Documentation Center
5010 Duke Street
Cameron Station
Alexandria, VA 22314

Copies 5 through 16